J. Fluid Mech. (1998), *vol.* 371, *pp.* 21–58. Printed in the United Kingdom

Post-stall flow control on an airfoil by local unsteady forcing

By JIE-ZHI WU, XI-YUN LU†, ANDREW G. DENNY‡, MENG FAN¶ AND JAIN-MING WU

The University of Tennessee Space Institute, Tullahoma, TN 37388, USA

(Received 14 January 1997 and in revised form 21 April 1998)

By using a Reynolds-averaged two-dimensional computation of a turbulent flow over an airfoil at post-stall angles of attack, we show that the massively separated and disordered unsteady flow can be effectively controlled by periodic blowing–suction near the leading edge with low-level power input. This unsteady forcing can modulate the evolution of the separated shear layer to promote the formation of concentrated lifting vortices, which in turn interact with trailing-edge vortices in a favourable manner and thereby alter the global deep-stall flow field. In a certain range of post-stall angles of attack and forcing frequencies, the unforced random separated flow can become periodic or quasi-periodic, associated with a significant lift enhancement. This opens a promising possibility for flight beyond the static stall to a much higher angle of attack. The same local control also leads, in some situations, to a reduction of drag. On a part of the airfoil the pressure fluctuation is suppressed as well, which would be beneficial for high-α buffet control. The computations are in qualitative agreement with several recent post-stall flow control experiments. The physical mechanisms responsible for post-stall flow control, as observed from the numerical data, are explored in terms of nonlinear mode competition and resonance, as well as vortex dynamics. The leading-edge shear layer and vortex shedding from the trailing edge are two basic constituents of unsteady post-stall flow and its control. Since the former has a rich spectrum of response to various disturbances, in a quite wide range the natural frequency of both constituents can shift and lock-in to the forcing frequency or its harmonics. Thus, most of the separated flow becomes resonant, associated with much more organized flow patterns. During this nonlinear process the coalescence of small vortices from the disturbed leading-edge shear layer is enhanced, causing a stronger entrainment and hence a stronger lifting vortex. Meanwhile, the unfavourable trailing-edge vortex is pushed downstream. The wake pattern also has a corresponding change: the shed vortices of alternate signs tend to be aligned, forming a train of close vortex couples with stronger downwash, rather than a Kármán street.

1. Introduction

Owing to the obvious importance in applications, a great effort has been made in the past two decades to enlarge the range of usable angles of attack for a large-

† On leave from Department of Modern Mechanics, University of Science and Technology of China, Hefei, Anhui 230026, China.

‡ Present address: Arnold Engineering Development Center, 740 4th Street, Arnold AFB, TN 37388-6001, USA.

¶ On leave from State Key Laboratory for Turbulence Research, Peking University, Beijing 100871, China.

aspect-ratio wing through various flow controls. Basically, relevant works fall into two categories. The first category is usually referred to as *separation control*, which concentrates on partially separated flow at $\alpha < \alpha_{stall}$, where α_{stall} is the static-stall angle of attack. Since the first experimental study of Collins & Zelenevitz (1975), there has been ample literature showing that a partially separated flow can become an almost fully attached flow by unsteady forcing, so that the stall is delayed. In this category, unsteady controls are much more effective than steady ones and can be realized at a very low power-input level (e.g. Wu, Vakili & Wu 1991; Seifert *et al.* 1993; Seifert, Darabi & Wygnanski 1996; Wygnanski 1997).

The second and more ambitious category is the *separated-flow control* after the flow has eventually fully separated. As α increases beyond α_{stall}, fully separated flow develops and becomes a bluff-body flow. This flow gives a normal force on the airfoil with a lift component, which reaches a peak at a maximum utilizable angle of attack, $\alpha_m \simeq 40^\circ$. This second peak can be of the same level as, or even higher than, the first one at α_{stall}. Meanwhile, drag also quickly increases (e.g. Fage & Johansen 1927; Critzos, Heyson & Baswinkle 1955).

Early experimental studies and physical analysis on separated-flow control, aiming at utilizing the whole range of $0 < \alpha < \alpha_m$ for a wing or flap, have been conducted by several groups and has a long history, as extensively reviewed by Wu *et al.* (1991). Based on the work of J. M. Wu and A. D. Vakili in the mid 1980s, these authors concluded that, first, the lift enhancement on a large-aspect-ratio wing should be the result of capturing a vortex on the upper surface of the wing in the time-averaged sense; and, second, since using steady controls cannot achieve this one must rely on unsteady controls with low-level power input. Wu *et al.* (1991) also conjectured that the underlying physics of post-stall lift enhancement by unsteady controls consists of a chain of mechanisms: vortex layer instability – receptivity – resonance – nonlinear streaming.

Experimental studies by Hsiao's group (Hsiao, Liu & Shyu 1990; Hsiao, Wang & Zohar 1993; Hsiao, Shyu & Chang 1994; Chang, Hsiao & Shyu 1992) using a NACA 63_3-018 airfoil, and Zhou and Fernholz (Zhou *et al.* 1993) using a NACA-0025 airfoil (with sharp edge forward), confirmed the above basic ideas. In a range of post-stall angle of attack up to about 35°, a local unsteady excitation (acoustic and/or oscillating flap) near the leading edge may increase the lift by 40% to 70%, and the lift/drag ratio can be increased up to 80% at a moderate α. The possibility of capturing a vortex by unsteady control was also confirmed analytically by Chernyshenko (1995). He used a simple theoretical model to prove that while a vortex above a circular cylinder in an oncoming flow is unstable and must move away, it can be stabilized and captured in the mean sense by a two-point alternate blowing–suction. Numerically, Laurie & Farokhi (1993) applied an inviscid discrete vortex method to compute the control effect by an oscillating leading-edge flap on the flow over a NACA-0012 airfoil at $\alpha = 15^\circ$. The flap has a chord length about $c/4$ and forms an upstream extension of the airfoil. The authors found that with forcing the lift is greatly increased. Then, passive control of turbulent separated flow over a NACA-0012 airfoil at $\alpha = 18^\circ$ was computed by Gillam & Cooper (1994) with the Baldwin–Lomax turbulence model. The control device consisted of a porous region and plenum located downstream of the mid-chord. It was found that the passive control can eliminate flow fluctuation.

In spite of this positive progress, a thorough understanding of the wing flow at a post-stall angle of attack and its control is still lacking due to the complexity of the flows. At such a large angle of attack shear layers are shed from both leading and trailing edges of the wing, rolling up into mutually interacting vortices. Secondary

and tertiary separations from the mid-portion of the upper surface may also be induced. All these make the flow field inherently unsteady, and no simple analytical theory is possible. Therefore, a full clarification of the mechanisms of post-stall lift enhancement by unsteady controls is highly desirable, which heavily relies on careful numerical simulations and detailed experimental flow-field surveys.

Motivated by the above needs, we carried out a series of two-dimensional Navier–Stokes computations of a post-stall turbulent flow over an airfoil and its unsteady control. The purpose of the study was twofold: to reproduce the lift and drag characteristics of uncontrolled and controlled flows, and to further clarify the physical mechanisms therein.

2. Physical background of post-stall flow control

We first discuss the basic physical mechanisms behind the post-stall flow control, which provides some guidance to our computation.

2.1. *The vortical source of post-stall lift and drag*

It is well known that, at least at low Mach numbers, lift (and drag) on a wing with attached flow is entirely due to the vorticity contained in asymmetric boundary layers on the upper and lower surfaces of the wing. Recently, Wu & Wu (1996) re-emphasized this vortical source of aerodynamic force by explicitly putting the Kutta–Joukowski lift formula (a counterclockwise circulation Γ is assumed positive)

$$L = -\rho U \Gamma \tag{1}$$

and its three-dimensional extension on the basis of viscous rotational flow theory. They show that these formulas hold if the flow is incompressible and steady, and if the Reynolds number approaches infinity (i.e. the 'Euler limit' of Navier–Stokes flow). In a fully separated unsteady flow, which is our concern, although the favourable circulation in the upper-surface boundary layer is mostly lost, (1) still holds in a time-averaged sense if the mean Γ of the whole flow field can be properly estimated. In the Kirchhoff–Rayleigh theory (Lamb 1932), the circulation in (1) already exists implicitly, because the free streamlines shed from the leading and trailing edges of an inclined flat plate are simply vortex sheets, or the Euler limit of shear layers. But the theory underestimates the normal force. In fact, once an airfoil starts to move at a post-stall angle of attack, the separated vortex sheets must immediately roll up at their free ends. They never have a chance to extend to infinity smoothly as assumed in Kirchhoff's theory. After the vortex sheets roll into concentrated vortices, they carry more favourable circulation above a wing with a low-pressure core compared to unrolled sheets (Wu & Wu 1993), and produce a higher normal force than that predicted by the Kirchhoff–Rayleigh theory. In other words, the difference between Kirchhoff's and Rayleigh's theoretical prediction and the experimental value of the normal force is a measure of the net contribution of vortex-sheet rolling up.

Roughly speaking, in the Euler limit a time-averaged separated flow can be viewed as a Prandtl–Batchelor flow with constant vorticity in a captured closed bubble or bubbles (Batchelor 1956). If the dimensionless bubble area and vorticity therein are S and ω_0, then by (1) the additional lift coefficient due to a vortex bubble is $C_l \simeq 2\omega_0 S$, and for the drag $C_d \simeq 2\omega_0^2 S/Re$ (Chernyshenko & Castro 1993). Thus, as ω_0 increases as α, the drag will increase even faster; and the lift/drag ratio $L/D \simeq Re/\omega_0$ increases as the Reynolds number.

From the above simple observation one may already learn something important about post-stall flow control. First, one should enhance the rolling up of the leading-edge shear layer (Wu & Wu 1993), such that the circulation above the wing is even larger than that in the attached boundary layer. This implies that the control should promote the discretization of this layer into individual vortices, and enhance their merging.

Secondly, since kinematically the total circulation (including the circulation carried away by wake vortices) in the flow field must be zero, the formation of unfavourable trailing-edge vortices is inevitable. But, what one could do through control is to suppress the rolling up of the trailing-edge shear layer and/or push the trailing-edge vortex downstream.

2.2. *Unforced randomness vs. forced resonance in separated flow*

We now examine the specific dominating mechanisms involved in post-stall flow control. Obviously, two major mechanisms must play an essential role in a fully separated flow field: the *local instability* of separated shear layers from both leading and trailing edges, and the *global instability* that causes vortex shedding. While the control of the former has benefited from the studies of forced mixing layers (e.g. Ho & Huerre 1984), that of the latter has benefited from the studies of forced cylinder-wake flows (e.g. Rockwell 1990). What we need is to combine these to guide our physical understanding and numerical tests.

2.2.1. *Unforced separated flow*

The dimensionless shear-layer frequency is defined as

$$St_{shear} = \frac{f_{shear}\theta}{\overline{U}}, \quad \overline{U} = \tfrac{1}{2}(U_1 + U_2), \tag{2}$$

where θ is the momentum thickness of the layer and U_1 and U_2 the velocities at its two edges. For different U_1 and U_2, the most unstable mode of an unforced straight shear layer always occurs at $St_{shear} \simeq 0.032$ if the flow is laminar, and $St_{shear} \simeq 0.044$–0.048 if the flow is turbulent (Ho & Huerre 1984). This most unstable frequency is referred to as the natural frequency and denoted by f^0_{shear}. Note that θ is an increasing function of the streamwise distance from the separation point, say s; hence, f^0_{shear} must be a decreasing function of s.

On the other hand, the global instability that causes vortex shedding is the result of absolute instability (e.g. Huerre & Monkewitz 1990). Therefore, owing to the coexistence of a variable f^0_{shear} and a natural shedding frequency f^0_{shed} between the leading-edge shear layer and trailing-edge vortices, plus the fluctuating frequencies of secondary and tertiary separations, the unforced separated flow must be a highly nonlinear multi-frequency system. In the system the shear-layer evolution and vortex shedding process are already coupled with and modulate each other. Because the interaction of three frequencies that are not mutually integer multiples of each other implies chaos, an unforced separated flow often exhibits random behaviour.

2.2.2. *Forced shear layer*

For a forced shear layer, the key parameter is the forcing frequency f_e. The response frequency of the shear layer, f^r_{shear}, may differ from f^0_{shear} and is shifted to a super- or subharmonic of f_e. Under this f^r_{shear}, the shear layer rolls up into discrete vortices, which then merge into larger ones with the characteristic frequency accordingly reduced. This process may continue in a stepwise manner, leading to a

rich spectrum of response to various disturbances. The merging process also enhances the entrainment. Such a *subharmonic resonance* and *frequency lock-in* are known to be the basic mechanism for effective shear-layer control, which always leads to a more regularized flow field than the non-resonant case.

In addition, a forcing at the very low frequency of $O(10^{-1}f^0_{shear})$ and a finite amplitude may cause the so-called 'forced fusion' (Rockwell 1972) or 'collective interaction' (Ho & Nosseir 1981; Ho & Huang 1982), in which a coalescence of many small vortices into a large one occurs within a short distance. Unal & Rockwell (1988) have proposed that this mechanism is responsible for the vortex formation from separated shear layers in a bluff-body flow. This could also be especially valuable for lift enhancement, because the length scale of a fully separated flow is usually not large enough for the formation of a large lifting vortex merely from successive pairings. On the other hand, unlike the straight shear layer appearing in the experiments of Rockwell and Ho and co-workers, the leading-edge shear layer above an airfoil has a tendency to turn down and roll up. This makes multi-vortex coalescence occur more easily under proper control. Because there is no absolute distinction between a perturbed shear layer and its discrete version, in what follows we shall name this phenomenon *rolling-up coalescence*.

2.2.3. *Forced vortex shedding and unsteady control*

After the controlled leading-edge shear layer is quickly discretized and a strong lifting vortex is formed by merging, the lifting vortex will interact with trailing-edge vortices just like in a bluff-body flow. Here we also have the frequency lock-in phenomenon, where the natural shedding frequency shifts to a harmonic of f_e (e.g. Stansby 1976). It is therefore possible to find a proper range of f_e so that the leading-edge and trailing-edge vortices are both effectively modulated by a *single forcing*. In fact, this possibility is reinforced by the following observation. While the momentum thickness θ of a laminar shear layer varies as $Re^{-1/2}$, that of a turbulent shear layer varies as $Re^{-1/7}$ (e.g. White 1974). Thus, if Re changes from 10^4 to 10^7, say, f^0_{shear} will increase by about 30 times for laminar flow but only about three times for turbulent flow. Due to the weak dependence of f^0_{shed} on Re (except the transition from subcritical to supercritical regimes), then, in turbulent flows the ratio f^0_{shear}/f^0_{shed} keeps the same order of magnitude in a wide range of Re. Actually, we found that $f^0_{shed}/f^0_{shear} = O(10^{-1})$. On the other hand, we are most interested in a forcing with $f_e = O(10^{-1})f^0_{shear}$ for promoting rolling-up coalescence. Therefore, a single forcing has a good chance of being effective.

Moreover, since disturbances can propagate both upstream and downstream in an absolutely unstable zone, there can be a natural mechanism to close the loop of resonance. In such a resonant flow the unfavourable random modes are suppressed, making the retained main modes very regular and strong.

From the above discussion it is clear that, unlike the wake control of a circular-cylinder flow, we now have to pay more attention to the flow field above the airfoil. In particular, the focus must be on the control of the leading-edge shear layer. Its upstream location and highly flexible receptivity, as well as the fact that it is the only source of lift, make the leading-edge shear layer the most effective constituent to be controlled. Obviously, for an effective control of such a shear layer the forcing must be imposed asymmetrically relative to the airfoil configuration, as in the case in the above-mentioned experiments with a single leading-edge control device. It should be stressed that the recent rapid development of smart materials and micro-fabricated electromechanical systems (MEMS) has made the desired unsteady active control

practically feasible without using any complex mechanical actuators (e.g. McMichael 1996).

3. Numerical method

3.1. *Numerical scheme*

A compressible Navier–Stokes solver was adapted to the present problem. The scheme is approximately factorized, using second-order central differencing in space plus a fourth-order artificial viscosity, and is second-order implicit in time. The code has been confirmed to work well at low Mach numbers by several test cases, including flow over a circular cylinder with vortex shedding, as well as attached and separated airfoil flows (Denny 1997). For the calculation performed in this study, an O-grid was employed and stretched such that the mesh height adjacent to the wall is less than 10^{-4}.

The computation is very complicated if it is to faithfully simulate an oscillating flap, where a moving grid has to be embedded in a fixed global grid. Such a computation has been carried out (Denny 1997) and will be reported elsewhere. In the present study we used local periodic blowing–suction located at 2.5% chord lengths from the leading edge to mimic the effect of forcing. This location has been shown by the experiments of Hsiao *et al.* (1993, 1994) to be most effective over a wide range of angle of attack. We stress that in this study the blowing–suction with no net flux is merely a simplified simulation of various control means; it cannot reflect the full effect of, say, an oscillating flap or some other specific device. But, periodic blowing–suction itself may well be a candidate for practical devices (e.g. Seifert *et al.* 1996), which could be achieved by using a synthetic jet (e.g. Smith & Glezer 1997), say, and does not require a complex system of pumps and pipes. Moreover, no matter what kind of specific actuator it is produced by, as long as the forcing disturbance has the proper frequency and amplitude, qualitatively the same end result could be anticipated.

The no-slip and impermeability conditions were imposed on the airfoil surface except at a few grid points at the blowing–suction location. A non-reflective condition (Thompson 1990) was imposed on the outer boundary of the computational domain. The initial condition was simply taken as a uniform flow. After starting, the transient state evolves to a quasi-periodic state. Data were recorded after the quasi-periodic state was reached.

The computational domain has a radius of 12 chord lengths, which was deemed sufficient by numerical tests. It has also been determined that the computed results are independent of the time step we used (or CFL number). In table 1 we show the time-averaged lift and drag coefficients, C_l and C_d, of a NACA-0012 airfoil along with their root-mean-square values, as well as the lift/drag ratio L/D, for a set of parameters with two grid resolutions, i.e. 141×181 (circumferential $\times$ normal) and 181×261. Because for this kind of massively separated and unsteady flow the initial transient stage is quite random and has a profound effect on the detailed fluctuating history of the flow, it is impractical to reach an exact grid independence. Thus, we judge our results for the two grid resolutions as in good agreement. In what follows we only show the results with 141×181 meshes.

3.2. *Parameters*

The computation focused mainly on the effect of forcing frequency and angle of attack; in several runs the amplitude effect was also examined.

In the experiments of Hsiao's group (Hsiao *et al.* 1990, 1993, 1994; Chang *et al.*

Grid	f_e/f_s	C_l	C_d	L/D	C_{lrms}	C_{drms}
141	0	1.017	0.543	1.873	0.295	0.138
181	1.0	1.540	0.551	2.795	0.302	0.230
181	0	1.046	0.559	1.871	0.316	0.149
261	1.0	1.576	0.578	2.727	0.293	0.221

TABLE 1. Validation of grid resolution: NACA-0012, $\alpha = 25^\circ$, $Re_c = 5 \times 10^5$. C_l, C_d, L/D are averaged values; C_{lrms}, C_{drms} are RMS values.

1992), it was reported that the forcing frequency was chosen as the shear-layer frequency f^0_{shear} for lower post-stall α, and the natural shedding frequency f^0_{shed} for higher α. Because θ and $\overline{U}$ in (2) vary along a streamline, and because above an airfoil the separated shear layer is no longer straight and there can be secondary and tertiary separations, how to select a single reference value of f^0_{shear} is not trivial (Hsiao *et al.* did not explain where the shear-layer frequency was detected). If f^0_{shear} was referred to the initial frequency at separation point, taking $f_e = f^0_{shear}$ might not be the best choice. In contrast, in the experiment of Zhou *et al.* (1993) it was found that the optimal effect occurred when $f_e = f^0_{shed}$ and its first superharmonics. Because the natural vortex-shedding frequency can be accurately determined by computation or experiment, it is more convenient to use f^0_{shed} as a reference in choosing our f_e. We thus define a relative forcing frequency

$$\widehat{f}_e = \frac{f_e}{f^0_{shed}}, \tag{3}$$

and for most runs we chose

$$\widehat{f}_e = 2^j, \quad j = 0, \ \pm 1, \ \pm 2, \ldots, \tag{4}$$

such that the imposed f_e can effectively modulate the vortex shedding process. As addressed before, in a range of angles of attack it is possible that $\widehat{f}_e$ given by (4) also falls into a proper range that can promote the vortex discretization in the shear layer and their merging.

We chose the Reynolds number Re_c (based on chord length c) as 5×10^5. This is of the same order as those in the experimental studies cited above (up to 6.7×10^5) (Zhou *et al.* 1993) and in the computation of Ko & McCroskey (1997), which was 6×10^5. The Mach number was fixed at 0.2. The airfoil for computation was NACA 0012, since its uncontrolled force character over the whole range of $0^\circ \leqslant \alpha \leqslant 360^\circ$ has been extensively studied by careful experiments (Critzos *et al.* 1955). But, this is certainly not the optimal shape for post-stall control purposes.

The periodic blowing–suction was simulated over five grid points of total length $l = 2.5\%c$ to form a velocity profile $v(s)$. The flow rate, defined by

$$c_\mu = \frac{|v|_{max} l}{Uc \sin\alpha}, \tag{5}$$

is fixed to 2.5% in most runs, which at $\alpha = 25^\circ$ corresponds to $|v|_{max}/U \simeq 0.42$. Introducing the factor $\sin\alpha$ is to ensure that with the same c_μ a higher α requires a larger $|v|_{max}/U$ as it should. This magnitude order of $|v|_{max}/U$ is relatively large in practice; the forcing effect with smaller amplitudes will be reported in § 4.1.2. It should be stressed that, the required c_μ may well be reduced by using a smaller l (for that case a denser grid would be needed) while keeping the same $|v|_{max}$. Chang *et al.* (1992)

have presented evidence that it is not the nominal c_μ but the maximum disturbance velocity $|v|_{max}/U$ that is crucial for the control.

3.3. *Turbulence models*

In Reynolds-averaged computations of separated unsteady turbulent flow, to find a proper yet simple turbulence model is an extremely delicate issue. These kinds of flows are very sensitive to the location of the separation point, initial transition point, and turbulence strength at the separation, etc. These quantities in turn strongly depend on the airfoil geometry and the Reynolds number. While for a circular-cylinder flow there is a well-defined category of flow regimes versus Reynolds number (e.g. Williamson 1996 and references therein), establishing a similar category for post-stall airfoils would be much more complicated. In a preliminary survey of existing experiments and computations on post-stall airfoil flow, we have found indications that, for a given airfoil, different flow regimes could occur depending on Reynolds numbers and angles of attack, as well as the airfoil geometry. There is quasi-periodic flow with regular vortex shedding; there can be unsteady flow with a very small Strouhal number (about $O(10^{-1})$ of that in a bluff-body flow); and, surprisingly, the turbulent flow could even converge to a steady state with a stationary vortex being completely captured above the airfoil. Figure 1 sketches this survey for the NACA-0012 airfoil, which includes some laboratory experiments and numerical tests using the Spalart–Allmaras (S–A) turbulence model (Spalart & Allmaras 1992). Due to the lack of systematic experimental data, whether all these regimes do appear in practice is still uncertain, and the boundaries of these regimes are far from being clarified. The occurrence of these regimes seems to have a close relation with the existence of two competing types of separation described by Jones (1934): front separation and rear separation. While the former causes a stall with sudden increase in the fluctuations of lift and drag, the stall caused by the latter has no serious fluctuations. Which type will occur depends on the airfoil geometry very sensitively.

Because of this complexity, therefore, it could well happen that different turbulence models, as well as their different combinations with various numerical schemes, may lead to qualitatively distinct predictions for a massively separated flow. A theoretically higher-level turbulence model may not be better than a lower-level one for computing unsteady separated flow. For example, in computing dynamic stall, a comparative study of the Baldwin–Lomax (B–L) algebraic model (Baldwin & Lomax 1978), the S–A model, and a standard k–ϵ model has been made by Ko & McCroskey (1997), who concluded that the S–A model seems to be the best. But opposite evidence also exists. For a study of the effects on qualitative flow behaviour of viscosity, grid density, and treatment of boundary conditions (NACA-0012; up to $\alpha = 15^\circ$ only), see Barton & Pulliam (1984).

Being aware of this uncertainty, therefore, in most runs of this fundamental study we used the B–L model for simplicity, along with the Launder–Sharma (1974) wall-damping function. The B-L model is known to overestimate the lift for separated flow (Ko & McCroskey 1997). This was also observed in our computation (see §4.1 below). We did find that the S–A model gives somewhat better agreement with experimentally measured time-averaged forces (Denny 1997; Zhu 1997, private communication). However, the most puzzling problem is, at $Re = 5 \times 10^5$, that all flow patterns predicted by using the B–L model fall into the 'turbulent vortex shedding' regime of figure 1 for all our tested α, rather than the 'turbulent steady stall' regime predicted by using the S–A model for about $18^\circ \leqslant \alpha \leqslant 25^\circ$. As a comparison, we have computed the flow field at $\alpha = 20^\circ$ without any turbulence model for $Re = 10^5$

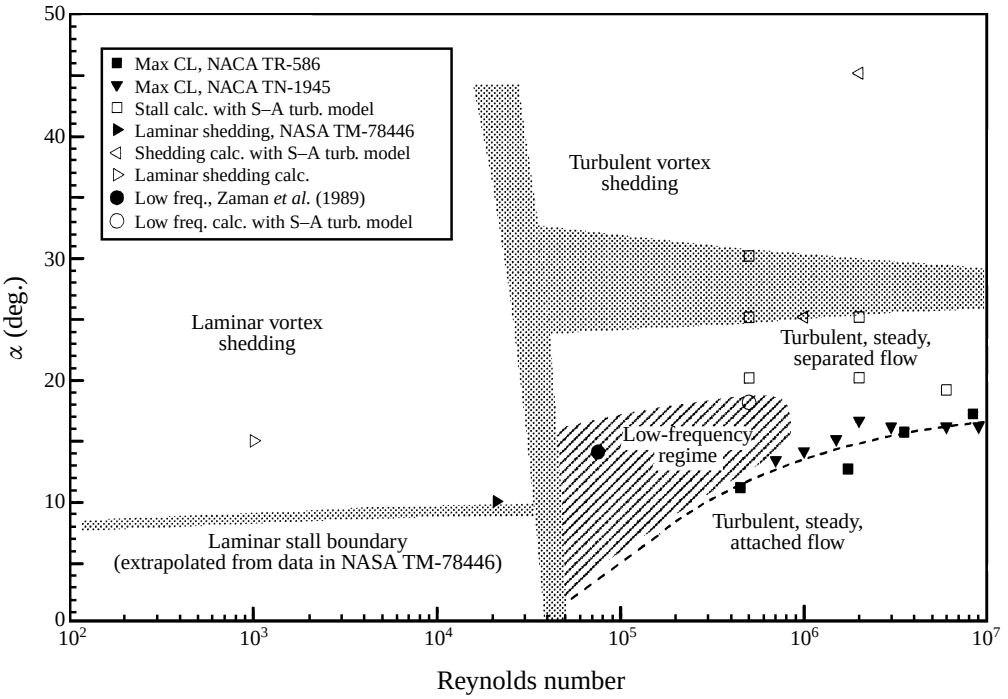

FIGURE 1. Possible regimes of flow patterns over a NACA-0012 airfoil at post-stall angles of attack versus Reynolds number. All data are taken from experiment unless noted. Shaded regions denote tentative approximate boundaries.

and 5×10^5 ('laminar' and/or 'transitional' flow). Both belong to the vortex shedding regime. A similar puzzle has been encountered by Rumsey *et al.* (1987) with the B–L model at $Re = 10^6$; they showed that at $\alpha = 18^\circ$ the flow is oscillating, but at $\alpha = 25^\circ$ it is steady. It is worth mentioning that we also met the sensitivity of post-stall flow (and/or turbulence models) to airfoil geometry: when applied to the NACA 63_3-018 airfoil, the same numerical code with the S–A model predicts oscillating flow at the same range of angle of attack and Reynolds number (Denny 1997). Denny also gave a more detailed discussion on the effect of turbulence models, grid density, artificial viscosity, and time step in post-stall flow simulation.

In effect, even for a two-dimensional airfoil, the real turbulent flow is inherently three-dimensional, with the wavelength of spanwise fluctuations comparable to the size of eddies that can be resolved by two-dimensional Reynolds-averaged computation. Moreover, small eddies formed from the disturbed shear layer could have an important effect on the evolution of massively separated flows and their controls, but they could have been smeared out by the Reynolds-averaged approach. Therefore, all two-dimensional computations at Reynolds-average level, including those listed in figure 1 and that in our study, by no means faithfully simulate these kinds of complicated flows. Rather, we hope to call more attention to this messy situation, which reflects an urgent need for systematically determining the boundaries between different regimes and justifying the practical applicability of various models (along with various schemes) by more reliable methods, e.g. accurate experiment or large-eddy simulation, etc.

Nevertheless, a three-dimensional turbulent post-stall flow is generically random

α (deg.)	f_e	C_l	C_d	L/D	C_{lrms}	C_{drms}
18	0	0.988	0.261	3.785	0.073	0.017
	0.5	0.952	0.227	4.194	0.149	0.042
	1.0	0.891	0.223	4.005	0.125	0.059
	2.0	0.987	0.233	4.236	0.084	0.035
	4.0	1.003	0.238	4.214	0.085	0.026
	8.0	0.989	0.242	4.087	0.091	0.028
20	0	0.968	0.388	2.495	0.194	0.052
	1/3	1.370	0.419	3.269	0.312	0.171
	0.5	1.395	0.397	3.514	0.294	0.149
	1.0	1.275	0.324	3.935	0.134	0.077
	1.5	1.042	0.296	3.520	0.120	0.075
	2.0	1.003	0.306	3.278	0.130	0.057
	4.0	1.066	0.338	3.154	0.116	0.048
25	0	1.017	0.543	1.873	0.295	0.138
	0.5	1.761	0.671	2.624	0.256	0.248
	1.0	1.540	0.551	2.795	0.302	0.230
	2.0	1.382	0.503	2.748	0.120	0.094
	4.0	1.187	0.488	2.432	0.150	0.084
30	0	1.125	0.729	1.543	0.299	0.162
	0.5	1.740	0.935	1.861	0.388	0.278
	1.0	1.714	0.919	1.865	0.427	0.299
	2.0	1.615	0.844	1.914	0.259	0.175
35	0	1.267	0.985	1.286	0.308	0.194
	0.5	1.457	1.083	1.345	0.412	0.277
	1.0	1.596	1.143	1.396	0.428	0.287
	2.0	1.696	1.226	1.383	0.372	0.226

TABLE 2. Time-averaged effect of forcing at different angles of attack and frequencies.

and unsteady. We thus believe that our results can at least be used for qualitative understanding of the underlying physics of most post-stall flows and their control. This is the main purpose of the present paper.

The computations were carried out on a Cray-C90 supercomputer. Each run took about 1–2 hours of CPU time. In the computation, the angle of attack was taken as 18°, 20°, 25°, 30° and 35°. Based on (3) and (4), a selective set of values of forcing frequency, $\widehat{f}_e = 0, 0.5, 1.0, 2.0$, and 4.0, was first tested at $\alpha = 25°$. Then the most effective values of f_e were tested for other α, where a few additional values of $\widehat{f}_e$ were also tested.

4. Lift, drag and pressure

4.1. *Lift and drag*

The computed time-averaged lift and drag at different α and f_e are compared in table 2, where the root-mean-square (RMS), amplitudes of C_l and C_d, are also listed. The computed lift enhancement is summarized in figure 2, where the experimental curve for unforced flow (Critzos *et al.* 1955) is also shown which is lower than the numerical result with $f_e = 0$. As mentioned before, this discrepancy is mainly due to the inaccurate turbulence modelling, and can be reduced by using better turbulence models. Nevertheless, figure 2 indicates that this overestimate occurs at all computed α, so the right trend of variation was nevertheless captured. The figure vividly

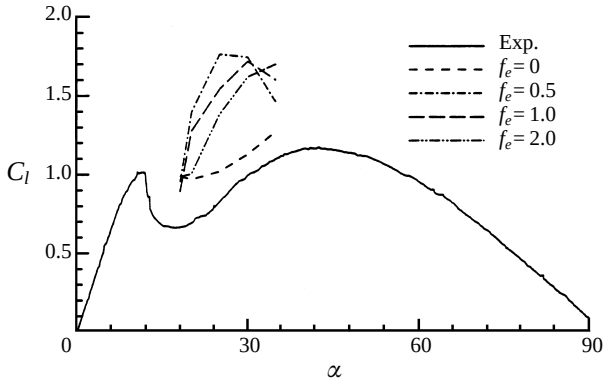

FIGURE 2. Overall view of mean lift enhancement due to forcing. NACA-0012 airfoil. Solid line is experimental value (Critzos *et al.* 1955).

indicates that, compared to the uncontrolled post-stall case, there is a significant lift enhancement up to $\alpha = 35°$. Only a narrow lift valley around $\alpha_{stall} \simeq 12°$ (for $Re_c = 5 \times 10^5$) remains, which has a width of about 7°. This residual valley could be eliminated by adding a high-frequency component in the forcing with $f_e \simeq f^0_{shear}$ (Seifert *et al.* 1996), or by sweeping the wing.

A similar effect of forcing was also observed at $\alpha = 20°$ and $Re = 10^5$ without any turbulence model: the mean lift coefficient was increased from the unforced value $\overline{C}_l = 1.25$ to 1.41 at $\widehat{f}_e = 1$, and the mean drag coefficient was decreased correspondingly from $\overline{C}_d = 0.46$ to 0.36. However, for $Re = 5 \times 10^5$, the same forcing seems to have no obvious effect on $\overline{C}_l$ and $\overline{C}_d$ if no turbulence model was turned on.

In what follows we examine some details of the effect of forcing frequency, amplitude and angle of attack.

4.1.1. *Effect of forcing frequency*

To illustrate the result, we fixed $\alpha = 25°$. In this case $f^0_{shed} = 0.152 f^0_{shear}$, where f^0_{shear} is estimated at a point just downstream of the separation point.

Figure 3(*a*) gives a typical time variation of lift and drag coefficients for the unforced flow. The corresponding power spectrum of C_l is shown in figure 3(*b*), where the only peak is at $St^0_{shed} = f^0_{shed} c/(U \sin\alpha) \simeq 0.158$, no other modes being excited. A quasi-periodicity is clearly seen, mainly modulated by the natural vortex shedding frequency. The time-dependent C_l and C_d under forcing, as well as their power spectra, are shown in figures 4–7. The following effects of forcing frequency are then evident.

First, *harmonic resonance with vortex shedding* obviously happens at $\widehat{f}_e = 1.0$ and 2.0 (figures 5 and 6). In both cases many harmonic modes of f^0_{shed} are excited. Consequently, we obtain the most favourable increase of lift/drag ratio (49.2% and 46.7%, respectively). In particular, the random high-frequency modes observed for the unforced case are almost completely suppressed when $f_e = 2f^0_{shed}$, implying a *perfect frequency lock-in*, which is the characteristic of the strongest resonance. This pattern must represent a well-organized vortical flow.

Secondly, the above two cases have very different amplitudes of C_l and C_d. While at $\widehat{f}_e = 1.0$ the amplitude is even larger than the unforced case, it is much smaller at $\widehat{f}_e = 2.0$. Figures 5(*a*) and 6(*a*) suggest that a dramatic change of the vortex shedding pattern takes place as the forcing frequency is doubled: one large vortex is replaced

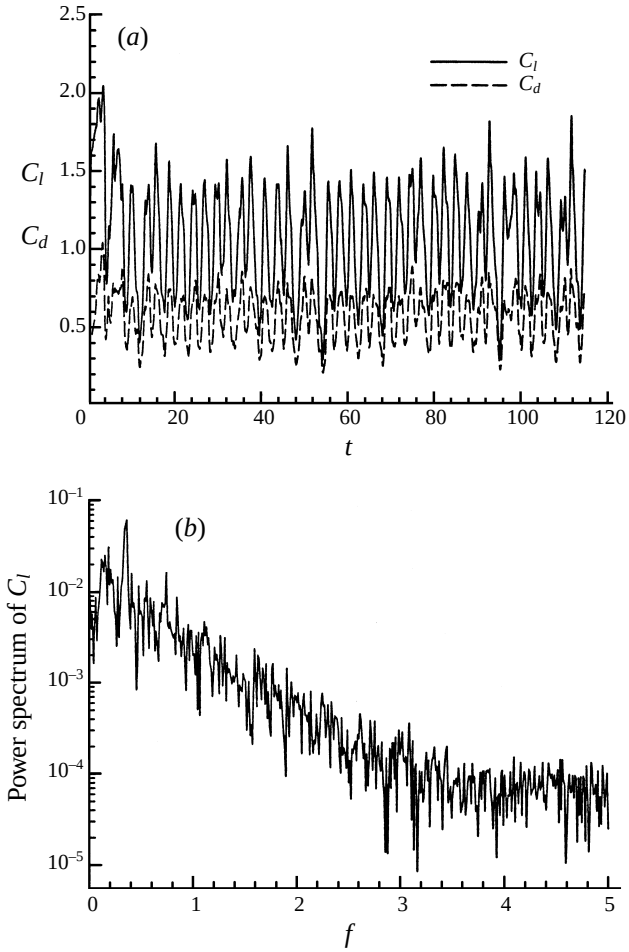

FIGURE 3. Unsteady force character of NACA-0012 airfoil. Unforced flow, $Re_c = 5 \times 10^5$, $M = 0.2$, $a = 25°$. The dimensionless time in this and following figures is Ut/c. (*a*) Instantaneous lift and drag coefficients. (*b*) Power spectral density of C_l.

by two smaller ones, which are shed at $\widehat{f}_e = 2.0$. Therefore, a resonant state is not necessarily associated with amplitude amplification. The same phenomenon has also been observed in circular-cylinder flow control (Lu & Sato 1996). In addition to a high lift/drag ratio, in practice the amplitude of C_l and C_d should be as small as possible.

Thirdly, as $\widehat{f}_e$ reduced to 0.5 (figure 4), we have *subharmonic resonance with vortex shedding*. This leads to the largest lift increase (73.2%) among all test cases, but the drag is also increased by 23.6% (the total normal force is increased by 41.8%). Many subharmonic modes are excited, but other modes are less suppressed compared to $\widehat{f}_e = 1$ and 2. On the other hand, the largest drag reduction (5.5%) occurs when $\widehat{f}_e = 4$ (figure 7), but the lift increase is small. Therefore, the optimal lift enhancement, drag reduction, lift/drag-ratio increase, and amplitude alleviation, all occurred at different forcing frequencies.

Finally, we stress that the selection of $\widehat{f}_e$ according to (4) is merely for convenience. It by no means implies that these discrete numbers are optimal. Actually, under a

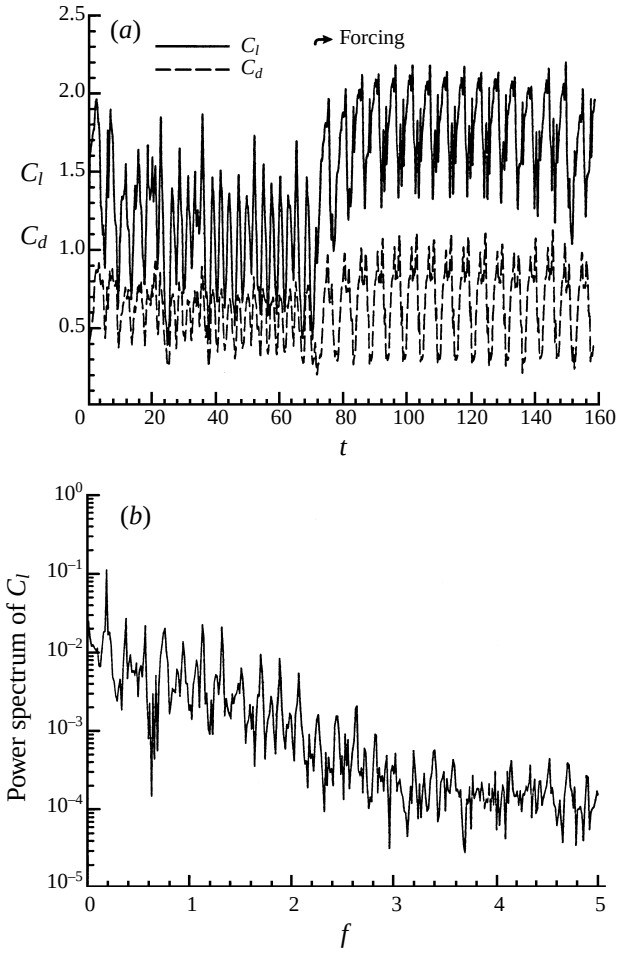

FIGURE 4. Forced flow. $\widehat{f}_e = 0.5$, $c_\mu = 2.5\%$. For other details see figure 3.

forcing the shedding frequency of a trailing-edge vortex must have a shift, being no longer f^0_{shed}. Moreover, we have also computed the case with $\widehat{f}_e = 1/3$ (table 2), $\sqrt{2}$, and $\sqrt{3}/2$ at $\alpha = 20^\circ$. The effect of $\widehat{f}$ on $\overline{C}_l$ and $\overline{C}_d$ is summarized in figure 8 for $\alpha = 20^\circ$, indicating that the effective frequency spans a wide smooth spectrum, which is very favourable in practical applications.

4.1.2. *Effect of amplitude*

The effect of amplitude, c_μ or v_{max}/U, was tested for several selected cases. At $\alpha = 25^\circ$ and $\widehat{f}_e = 1$, a forcing with $c_\mu = 1\%$ ($v_{max}/U \simeq 0.17$) has only a negligible effect on the lift. This is in qualitative agreement with the observation of Ho & Nosseir (1981) that the rolling-up coalescence is a nonlinear phenomenon that occurs only if the forcing amplitude is above a threshold value.

At a higher $\widehat{f}_e$, however, the rolling-up coalescence may not be able to occur; thus a forcing with a lower amplitude could be effective. We tested this at $\alpha = 20^\circ$ and $\widehat{f}_e = 1$ for several v_{max}/U (table 2 indicates that the peak lift enhancement that corresponds to possible rolling-up coalescence occurs when $\widehat{f}_e \simeq 0.5$). The result is

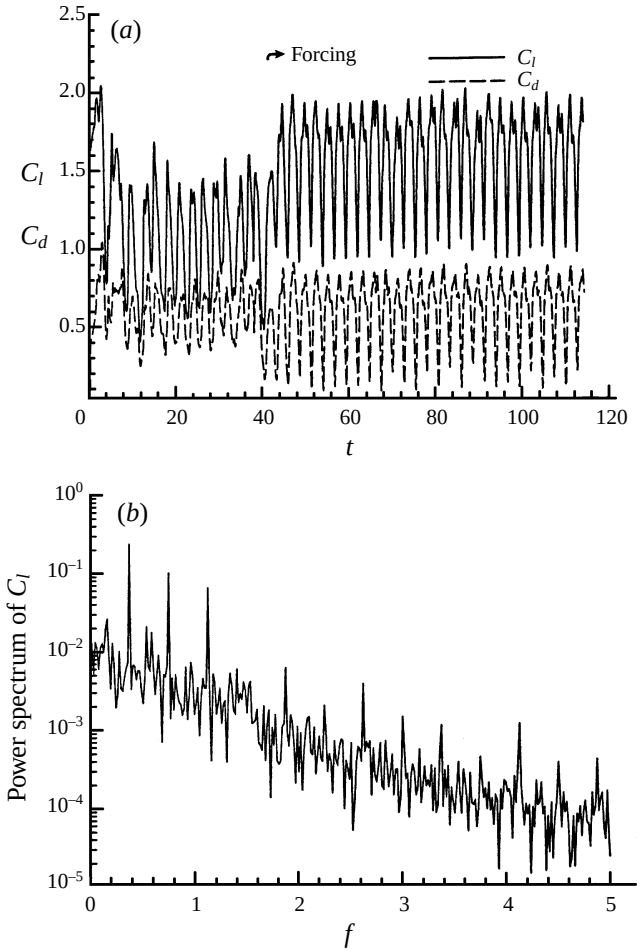

FIGURE 5. As figure 4 but $\widehat{f}_e = 1$.

shown in figure 9. The control effect is still nonlinear; but it seems that no clear-cut threshold amplitude exists. It was observed that when $v_{max}/U < 0.1$ the flow is no longer well organized, although the lift is still enhanced, even greatly, along with a drag enhancement.

Figure 9 suggests that the flow may have more than one response mechanism depending on the forcing amplitude. In the small-amplitude range both lift and drag are increased by the forcing as Hsiao's group observed, and reach a peak at an optimal amplitude, say v_{max1}. This range does not require a regularization of the flow, and the power input for effective control can be very small. But, the physics behind this effect is not yet very clear to us. In contrast, in the large-amplitude range, the flow is regularized, and the lift enhancement may be (not always) associated with a drag reduction. Although not seen from figure 9, a second peak of lift should exist at another optimal amplitude $v_{max2} \sim 10v_{max1}$. Most of our computations and discussion belong to this case, which, however, has never been observed in experiments. A systematic study of the amplitude effect at various angles of attack and forcing frequencies is therefore highly desirable.

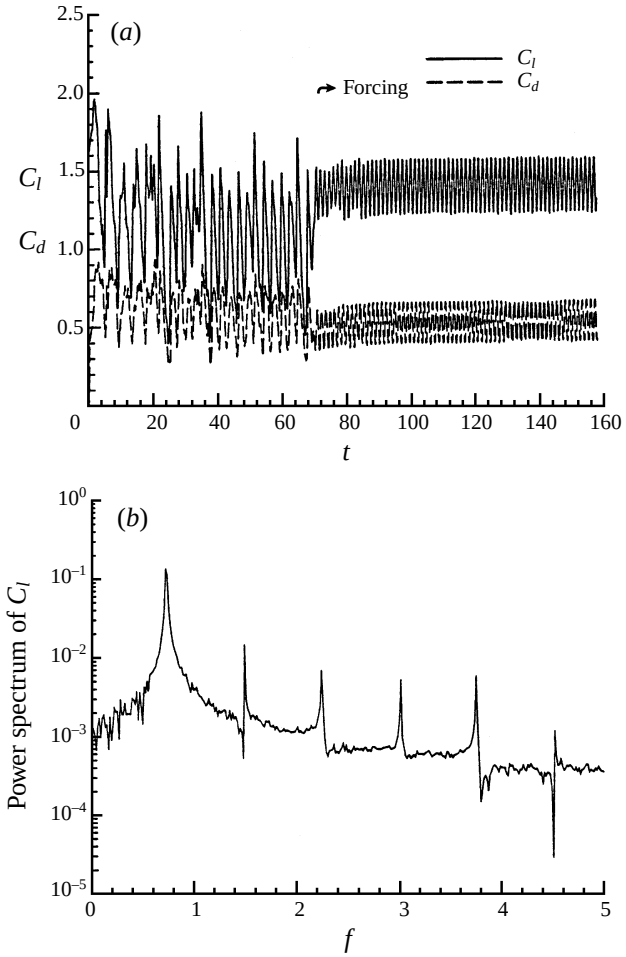

FIGURE 6. As figure 4 but $\widehat{f}_e = 2$.

4.1.3. *Effect of angle of attack*

At different angles of attack, similar pictures of C_l and C_d with various forcing frequencies were obtained. It is sufficient here to look at table 2 for the time-averaged values of lift, drag, and lift/drag ratio. The table also roughly outlines the range of angle of attack for effective flow control: between 20° and 30°. The strongest effect occurs at $\alpha = 20°$, where the optimal enhancement of the lift/drag ratio is as large as 57.7% at $\widehat{f}_e = 1.0$. Interestingly, this is also the frequency with an almost perfect lock-in phenomenon, similar to the case at $\alpha = 25°$ with $\widehat{f}_e = 2.0$.

The effect of unsteady control quickly drops to the level of 10% both as α decreases only 2° below 20°, and as α increases beyond 30°.

4.2. *Surface pressure*

We fix $\alpha = 20°$ as an example to look at the effect of forcing on surface pressure. Most runs used $c_\mu = 2.5\%$.

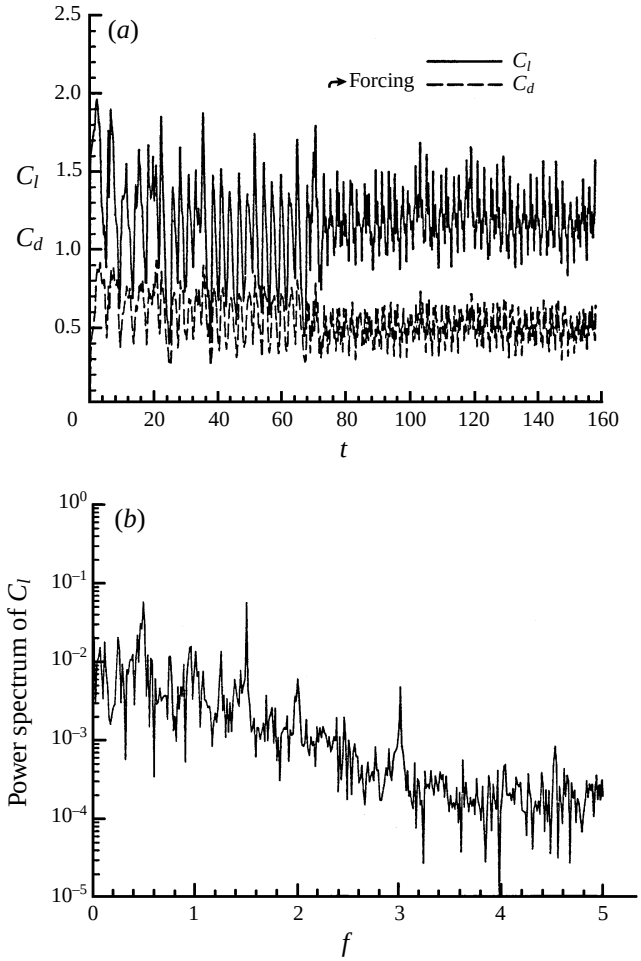

FIGURE 7. As figure 4 but $\widehat{f}_e = 4$.

4.2.1. *Response frequency and amplitude*

The instantaneous pressure distribution without forcing and with $\widehat{f}_e = 1$ at four different times of a cycle are shown in figure 10, and the RMS C_p fluctuations are shown in figure 11. Without forcing, a major part of the upper surface is in completely separated flow as indicated by the planform of the curves; and there is a strong C_p fluctuation near the trailing edge ($x/c > 0.85$). When the forcing is turned on, a strong lifting vortex travels above the upper surface and hence causes a moving suction peak. Moreover, the forcing almost entirely eliminates the unfavourable RMS peaks near the trailing edge, but the fluctuation on the front portion is enhanced. In particular, a very strong narrow RMS peak of C_p appears near the leading edge.

Figure 12 shows the time-dependent C_p and the corresponding power spectral density at $x/c = 0.9848$. Evidently, with forcing, the original broadband fluctuating frequency is locked-in to $\widehat{f}_e$ and its harmonics like C_l and C_d. On the other hand, the forcing reduces the C_p amplitude near trailing edge by eight times, but greatly enhances it near the leading edge (figure 11). The latter may be attributed to several mechanisms, of which we list two. First, because the periodic blowing/suction is a source of

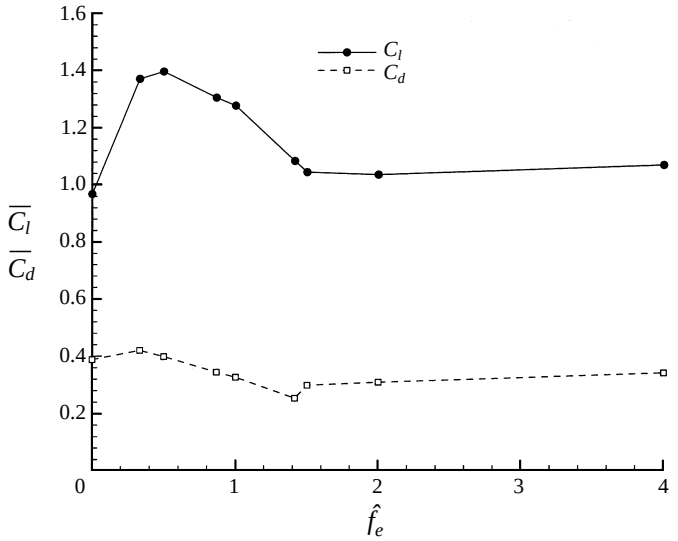

FIGURE 8. Time-averaged lift and drag coefficients against forcing frequency. $\alpha = 20°$, $c_\mu = 2.5\%$, $Re_c = 5 \times 10^5$.

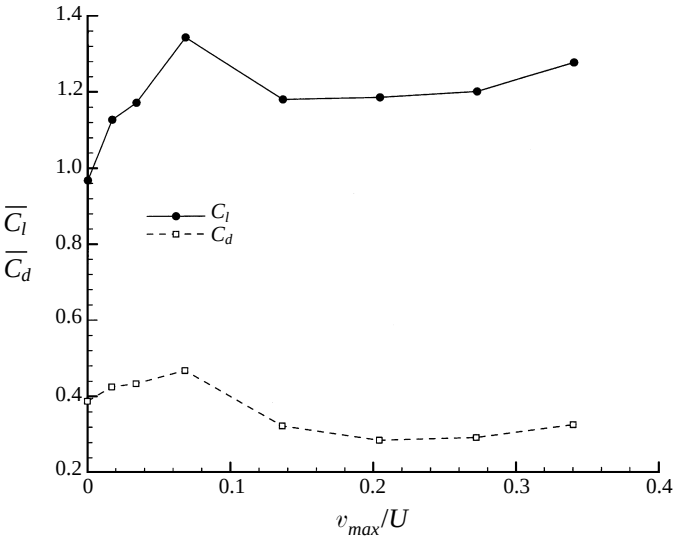

FIGURE 9. Time-averaged lift and drag coefficients against forcing amplitude, $\alpha = 20°$, $\hat{f}_e = 1$, $Re_c = 5 \times 10^5$.

pressure waves, in two-dimensional flow the C_p amplitude must have a contribution roughly inversely proportional to the distance from the forcing location and reaching a maximum near the leading edge. Secondly, and perhaps more importantly, in the forced flow the lifting vortices are strong and concentrated, and each shedding implies a strong impulse to the flow field compared to the unforced case where these vortices are much weaker and leave the airfoil quite randomly. Then these impulses may induce a stronger and more regularized oscillation of the separation point as well as of the kinetic energy contained in the separating boundary layer, which also occurs near the leading edge.

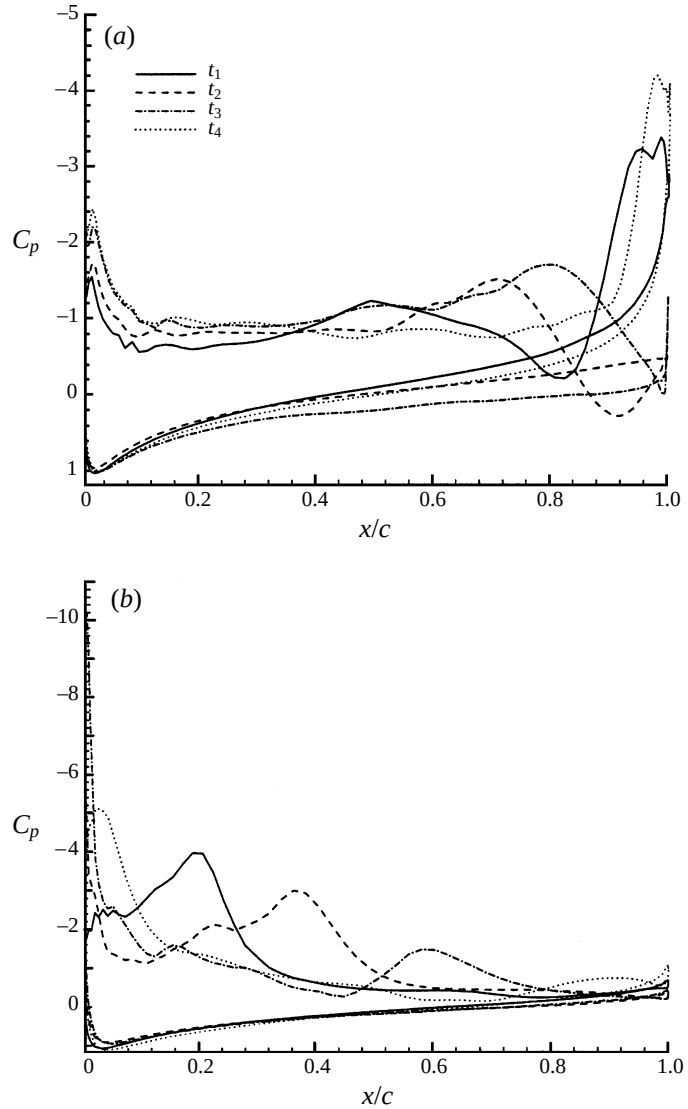

FIGURE 10. Time-variation of C_p distribution. $\alpha = 20°$. (*a*) Unforced. (*b*) Forced, $\widehat{f}_e = 1$, $c_\mu = 2.5\%$.

The above discussion, however, cannot fully explain why the strong RMS peak near the trailing edge is greatly suppressed by forcing. We leave this issue to § 6.2.

4.2.2. *Potential application in buffet control*

As suggested by V. Sharma (1996, private communication), the change of pressure character due to forcing may have potential benefit for buffet control, which requires minimizing the C_p amplitude and avoiding a broadband frequency spectrum. We saw that this goal has already been reached near the trailing edge. To reduce the amplitude in the front part, one could reduce c_μ to a minimum effective value. We found that when c_μ is decreased from 2.5% to 1.5%, the C_p amplitude can be reduced by 27% near the leading edge. Another possible means is to adjust $\widehat{f}_e$. A higher $\widehat{f}_e$ could spread the energy of a single strong impulse to several weaker ones. Setting

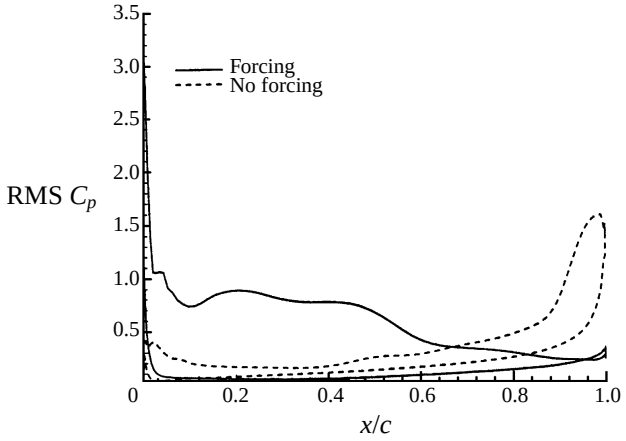

FIGURE 11. RMS C_p distribution. For other details see figure 10.

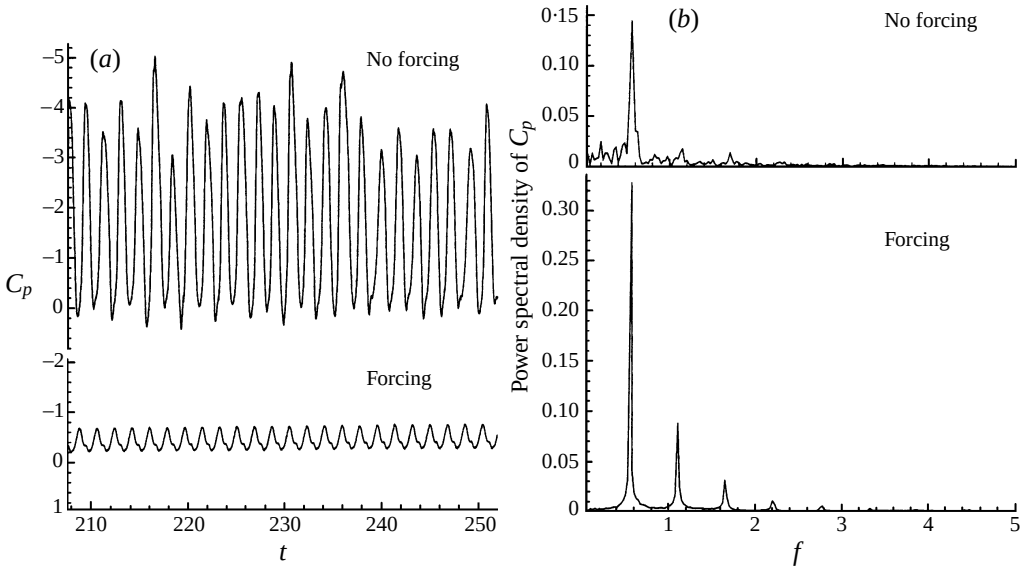

FIGURE 12. C_p fluctuation without and with forcing near the trailing edge. Flow conditions are as in figure 10. (*a*) Time-variation of C_p. (*b*) Power spectral density of C_p.

$\widehat{f}_e = 2$ confirmed this conjecture, where for the same $c_\mu = 2.5\%$ the leading-edge C_p amplitude is reduced by 12.8% compared to $\widehat{f}_e = 1$. An additional benefit is that the spacing between two neighbouring peaks is doubled, implying a smaller chance of exciting the buffet.

In addition, one could consider a different forcing mode. If instead of blowing–suction the forcing device only creates tangential oscillation along the wall, then the forcing wave will be a transverse wave (vortical wave), and the forced C_p fluctuation should be weaker. Theoretical studies have confirmed that this kind of transverse forcing mode can be applied to separation control (Wu, Wu & Wu 1991, 1993). Note that the vortical wave is also the source of a longitudinal pressure wave, but this effect is secondary (Wu, Ma & Wu 1994). Moreover, the phase difference effect between

forcing and responding waves is also worth exploring. Finally, a sharp leading edge with a fixed separation point would further reduce the separation oscillation. A numerical study based on these thoughts are being undertaken.

4.3. *Necessary conditions for post-stall flow control*

According to the discussion of § 2, in addition to the parameters and location of forcing, it seems that the following two basic conditions for post-stall lift enhancement are necessary: (i) the coexistence of a well-developed free shear layer and trailing-edge vortices; and (ii) a well shaped 'resonant cavity' enclosed by the leading-edge shear layer, trailing-edge vortices, and upper surface of the wing.

In the first condition, the shear layer must be free enough to undergo the local instability, discretization, and pairing, or rolling-up coalescence. Only in this case can these processes be effectively modulated by forcing. For α too close to α_{stall}, the shear layer is too close to the surface (as observed at $\alpha = 18^\circ$; the figure is not shown) and loses part of its freedom to be modulated. Thus, the forcing effect is reduced.

In the second condition, the above mentioned 'resonant cavity' cannot be too large. For otherwise the intrinsic communication between the shear layer and trailing-edge vortices will be too weak. This happens for $\alpha \geqslant 35^\circ$, and explains why the forcing effect declines at too large angles of attack. Note that this condition also emphasizes the importance of the airfoil shape.

5. Forced resonance and mode competition

Having obtained positive results for post-stall unsteady flow control by local excitation, we proceed to further explore the underlying physics. We first look at the flow as a nonlinear oscillator.

There is a basic difference between our study and most studies on mode competition and nonlinear interaction in bluff-body wake flows. While the latter have been based on experimentally measured data (e.g. Kourta *et al.* 1987) or direct numerical simulation at a laminar Reynolds number (e.g. Karniadakis & Triantafyllou 1989), our data were taken from Reynolds-averaged computations with an eddy-viscosity model, where small-scale fluctuations have been smeared out. Before going into detail, therefore, a general discussion is necessary to clarify in what sense the concepts of instability, coherent structure, and chaos can be applied to the Reynolds average of a turbulent flow.

The applicability of the concept of instability to fully developed turbulent flow lies in the existence of turbulent coherent structures. Successful attempts have been made to apply the linear instability theory, originally developed for laminar flow and transition, to predict the onset of coherent structures and their development (e.g. Wygnanski 1987). The prediction is improved by introducing a variable eddy viscosity into the Orr–Sommerfeld equation with slowly varying unidirectional basic flow, which is drawn from experiment by taking a time average. Thus, it has been established that turbulent flows also have an instability problem in an averaged sense, and between two statistical states, say a periodic one and a steady one, transition may happen due to the change of a parameter. Some necessary conditions for the stability of a statistically steady turbulent state have been found recently by Malkus (1996).

It is also meaningful, therefore, to talk about the instability of a Reynolds-averaged turbulent flow. The average should be understood as an ensemble average to allow for unsteadiness. Actually, using an eddy-viscosity model to simulate a Navier–Stokes

turbulent flow can be viewed as dealing with a laminar flow of a model fluid with a nonlinear constitutive structure; so the instability problem is always there.

The existence of nonlinear instability in a Reynolds-averaged turbulent flow, then, immediately implies the possibility that chaos may appear at large scales. Of course, this chaos must be distinguished from that leading to transition from laminar to turbulent flows. For a flow past an oscillating circular cylinder at a low Reynolds number, Olinger & Screenivasan (1988) have experimentally confirmed that the nonlinear interaction of two competing frequencies (forcing and shedding) can lead to chaos through quasi-periodicity, characterized by 'Arnold's tongues'. In this aspect, our situation is somewhat similar. We shall also see that, as the forcing frequency increases from zero, the transition takes place from unforced chaotic flow to forced periodic flow, and then to forced chaotic flow. In between the periodic and chaotic states there are some quasi-periodic states. Essentially, the chaos is due to the nonlinear interaction of different constituents of post-stall flows, each of which has its own characteristic frequency.

In a numerical study of unforced and forced laminar flow over a circular cylinder at $Re = 100$ based on cylinder diameter, Karniadakis & Triantafyllou (1989) assumed that the excitation provided by the shear-layer instability lies outside the receptivity region of the wake. Thus, in their computation only a single shedding frequency responded to the forcing frequency, which implies a quasi-periodic or periodic flow as they observed. The shear-layer instability in circular-cylinder flows was detected experimentally only at higher Reynolds numbers (above 350 by Gerrard 1978; and 1900 by Unal & Rockwell 1988). William-Stuber & Gharib (1990) observed chaos experimentally in the wake of a thin airfoil at $Re_c = 8600$. They set the airfoil at $\alpha = 0^\circ$ to remove the region of absolute instability, and used more than one active strip heater. Thus, two external excitations with different frequencies interact simultaneously with the shedding mode, which made the quasi-periodic pattern unstable and become chaotic.

In our case, the characteristic Reynolds number (based on chord length) is much higher, and the separated unstable shear layer from leading edge and its control play a crucial role in affecting the vortex shedding and wake. Therefore, many more high-frequency modes are excited. Chaotic regime appears as well as periodic and quasi-periodic ones. In this section, our focus is the conditions and results of different resonant states, frequency shift and lock-in, as well as a preliminary search of the periodic, quasi-periodic, and 'chaotic' regimes of the flow state. The types of unforced and forced flow patterns are summarized in table 3, a few typical details of which are addressed below.

5.1. *Unforced flow*

We first illustrate the flow behaviour using the data at $\alpha = 25^\circ$. Figures 13 and 14 give information about instantaneous velocity components (u, v) at two points in the unforced flow field, where plots (a) and (b) are respectively the phase diagram (velocity end-point diagram) and power spectral density (PSD) of the kinetic energy $(u^2 + v^2)/2$. As shown in the figure of table 3, point 1 is upstream of the airfoil, while point 2 is downstream of, and very close to, the leading-edge separation point. The fluctuation at point 1 is dominated by the global instability, so its PSD (figure 13b) has a single peak at a low f^0_{shed}. Figure 13(a) indicates that the flow at point 1 is more chaotic.

In contrast, point 2 is dominated by both f^0_{shed} and $f^0_{shear} = 6.60 f^0_{shed}$, as seen from figure 14$(b)$. Thus, the (u, v) fluctuation is much faster than that at point 1. The flow

α (deg.)	f_e/f^0_{shed}	f^r_{shed}/f^0_{shed}	Velocity pattern P1	P2	P3
20	1/3	1/3	P	P	Q
	1/2	1/2	Q	P	Q
	1.0	1.0	P	P	P
	3/2	3/2	C	P	Q
	2.0	7/6	C	P	Q
	4.0	4/3	C	P	Q
25	1/2	1/2	Q	Q	
	1.0	1.0	Q	Q	
	2.0	2.0	P	P	
	4.0	4/3	C	Q	
30	1.0	1.0	C	C	
	2.0	2.0	C	C	

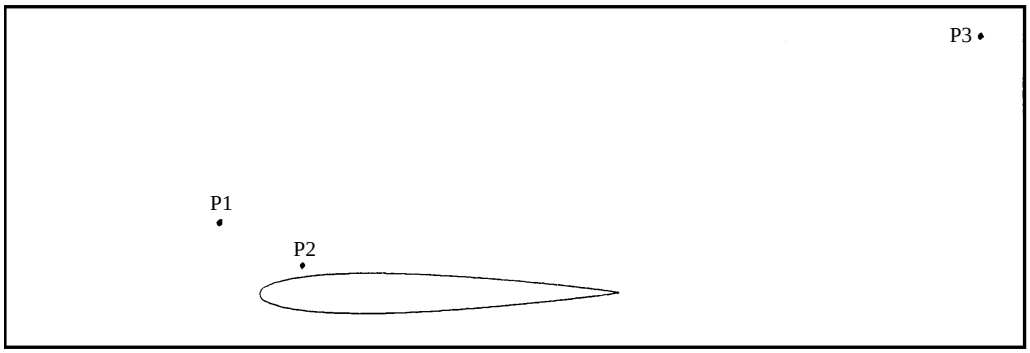

TABLE 3. Velocity patterns vs. α and f_e/f^0_{shed}. Location of points P1, P2, P3 are shown in the figure: $(x, y) = (-0.099, 0.213)$, (0.107, 0.074), (1.990, 0.775). P: Periodic. Q: Quasi-periodic. C: Chaotic.

is chaotic (figure 14*a*), and the corresponding PSD has broadband spectra. The waves around f^0_{shear} indicate that, at high Reynolds numbers, the leading-edge shear layer has a variable most unstable frequency (Ho & Huerre 1984). Therefore, as asserted in § 2.2, the unforced flow is already a multi-frequency system.

It has been found that the nonlinear interaction between two modes in high-Reynolds-number circular-cylinder flows is associated with the appearance of the sum and difference of two basic frequencies (e.g. Miksad *et al.* 1982). Kourta *et al.* (1987) use this mechanism to analyse the transition to turbulence in the wake of a cylinder. This phenomenon also appears in our case, as clearly seen from figure 14(*b*). Because the shedding mode has global influence, it interacts nonlinearly with local shear-layer instability modes. Except for a subharmonic peak at $f^0_{shed}/2$ at the low-frequency end, sum and difference modes were identified at

$$f^0_{shear} - 6f^0_{shed} = 0.6f^0_{shed}, \quad f^0_{shear} + f^0_{shed}/2 = 7.1f^0_{shed},$$
$$2f^0_{shear} - 6f^0_{shed} = 7.2f^0_{shed}, \quad 2f^0_{shear} - 5f^0_{shed} = 8.2f^0_{shed},$$

etc. The excitation of these sum and difference modes leads to the broadband waves and chaos.

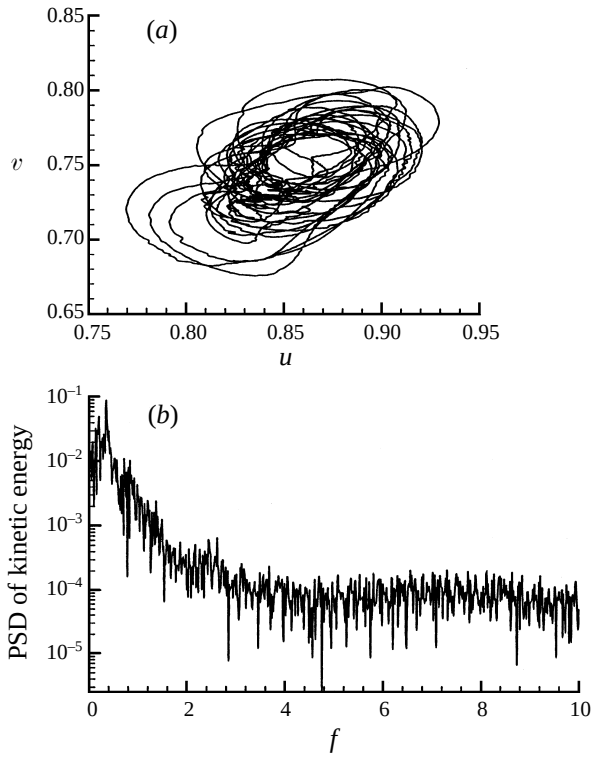

FIGURE 13. Instantaneous flow at point 1 of table 3. NACA-0012, $Re_c = 5 \times 10^5$, $M = 0.2$, $\alpha = 25°$. Unforced flow. (*a*) Phase diagram. (*b*) Power spectral density of kinetic energy $(u^2 + v^2)/2$.

We observed that the numerical result at $\alpha = 18°$ (not shown) exhibits a much more organized behaviour than that at $\alpha = 25°$. The flow-field survey indicates that at this lower angle of attack the leading-edge shear layer is very close to the airfoil surface, and can only develop much less unstable modes. Thus, the number of distinct frequencies taking part in interaction is reduced, and the flow at point 2 becomes quasi-periodic. On the other hand, increasing angle of attack to 30° will cause more variable unstable shear-layer frequencies to join the interaction, and hence more chaotic behaviour at the same point 2.

5.2. *Forced flow: frequency lock-in*

The most obvious effect of forcing on unsteady separated flow is that both response frequencies, f^r_{shed} and f^r_{shear}, lock-in to f_e and its harmonics as expected, which leads to a flow regularization, i.e. becoming quasi-periodic or periodic, as has been reflected by the force and pressure characteristics. This happens in a range of f_e, and the optimally organized patterns occur when

$$\alpha = 25° : \quad \widehat{f}_e = 2.0 = f^r_{shed} = \tfrac{1}{3} f^r_{shear},$$
$$\alpha = 20° : \quad \widehat{f}_e = 1.0 = f^r_{shed} = \tfrac{1}{6} f^r_{shear}.$$

Figures 15–17 show the results at points 1 and 2 for $\alpha = 25°$ and point 3 (downstream of the trailing edge, see the figure in table 3) for $\alpha = 20°$. These are in sharp contrast to figures 13 and 14.

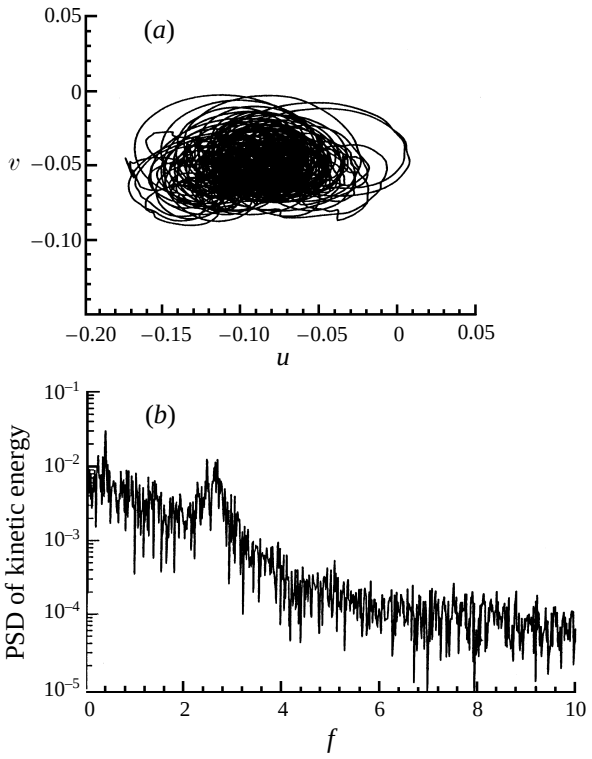

FIGURE 14. Instantaneous flow at point 2 of table 3. $\alpha = 25°$. For other details see figure 13.

Although the frequency lock-in has been found in bluff-body wake flows and airfoil flow at $\alpha = 0°$ (Koopmann 1967; Olinger & Sreenivasan 1988; Gharib & William-Stuber 1989; William-Stuber & Gharib 1990; Lam 1996), it is of interest that in post-stall airfoil flows it occurs in a much wider range of forcing frequency. This implies a better chance for control.

5.3. *Forced flow: frequency not lock-in*

As the forcing frequency increases beyond an upper bound, the shedding frequency no longer locks into f_e. At $\alpha = 20°$, this begins to be observed when $\widehat{f}_e = 2.0$. The non-lock-in of shedding frequency is most clearly seen at point 3 in the near wake, figure 18. The response shedding frequency becomes $f^r_{shed} = 7f_e/12 = 7f^0_{shed}/6$, which is a rational number close to the natural shedding frequency. Meanwhile, many superharmonics of $f_e/12$ are excited around f^r_{shed}; but only superharmonics of f_e remain at higher frequency range. Due to those $nf_e/12$ modes, the flow at point 3 is pseudo-periodic, but that at point 1 becomes more chaotic (not shown).

As mentioned before, shear layers are very flexible in responding to an external forcing, thus at $\alpha = 20°$ and $\widehat{f}_e = 2$ the shear-layer response frequency f^r_{shear} is still locked into nf_e and the flow near the leading-edge shear layer is still periodic.

As f_e further increases to $4f^0_{shed}$, for $\alpha = 20°$ we found that the response shedding frequency becomes $f_e/3 = 4f^0_{shed}/3$, again a rational number close to f^0_{shed}. Note that at point 3 (figure 19) there is a series of sideband peaks caused by a very low-frequency peak ($f_e/67$), implying a long-wave modulation of the flow. This long wave brings back the nonlinear interaction through the sum and difference modes,

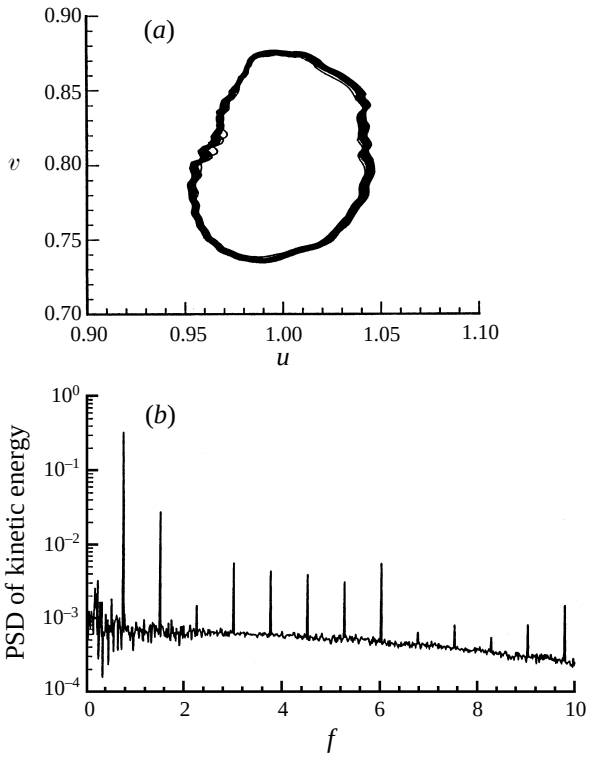

FIGURE 15. Instantaneous flow at point 1. $\alpha = 25°$, $\widehat{f}_e = 2$.

which was found to also modulate the integrated lift and drag (figure not shown). The same phenomenon in vortex shedding has been observed in some experiments and computations (e.g. Lu & Dalton 1996). It was checked that the $f_e/67$ peak is not due to the data sampling in a finite interval during Fourier transformation. It seems that this long wave is the result of f^r_{shed} drifting from $4f^0_{shed}$ and perfect lock-in has become impossible.

Similar non-lock-in of the response shedding frequency f^r_{shed} is also observed at $\alpha = 25°$ when $\widehat{f}_e = 4.0$. Once again, we have $f^r_{shed} = f_e/3$. The shear-layer response frequency is still a superharmonic of forcing.

6. Vorticity field and vortex dynamics

A forced nonlinear oscillator can represent many different physical systems. In order to fully understand the specific fluid-dynamic mechanisms of post-stall flow control, we must combine this kind of information with a flow-field survey. In this section, we display some instantaneous and time-averaged flow patterns at $\alpha = 25°$ and discuss their implications.

6.1. *Unforced versus forced instantaneous vorticity contours*

Figure 20 shows a few typical stages of vortex evolution in a period for unforced flow. We see a strong, well rolled-up trailing-edge vortex; some secondary and tertiary separated vortices from the mid-portion of the upper surface; and an irregularly drifting leading-edge shear layer. Only the last one is favourable for lift, but it

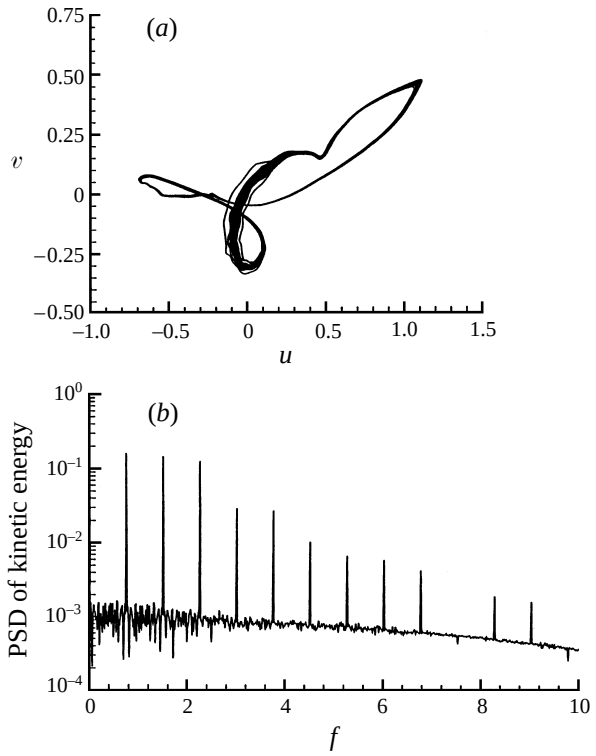

FIGURE 16. Instantaneous flow at point 2. $\alpha = 25°$, $\widehat{f}_e = 2$.

becomes two to three small discrete vortices (the location of their formation is random), and these favourable vortices are quite loosely associated with low-level vorticity. When the strong trailing-edge vortex stays above the rear part of the airfoil, the lift is minimum; while when it sheds away, the lift increases. The wake consists of a Kármán vortex street, though quite irregular, with an increasing width, in which the vortices of opposite signs are staggered.

The forced instantaneous vorticity contours at $\widehat{f}_e = 1.0$ are shown in figure 21. The leading-edge shear layer rolls up into a strong coherent favourable vortex nearer to the airfoil. In a smaller part of the period the secondary vortex still has an effect, but weaker than the unforced case. It is remarkable that the trailing-edge vortex shrinks to a narrow region and moves downstream before it sheds off. The wake vortices are now aligned in almost a single array. Such a single vortex array behind an oscillating airfoil has been observed by, e.g., Cornish (1982) and Koochesfahani (1989), and in an acoustically excited circular-cylinder flow by Detemple-Laake & Eckelmann (1989).

Note that the uneven spacing between the wake vortices of figure 21 implies that they form a row of short-spaced vortex couples rather than a Kármán street. Each vortex couple, which in the co-moving frame of reference appears as a Kelvin oval, carries along a body of fluid. Figure 22 sketches the patterns of the wakes for $\widehat{f}_e = 0$ and 1 (not to scale). For the unforced case, the wake flow induced by the vortices oscillates up and down, but in the mean sense has only a small downwash (see also figure 23*a* below). In contrast, for $\widehat{f}_e = 1$ the fluid carried by the vortex couples moves up; but since the spacing between neighbouring couples is larger, more fluid is induced to move down. Thus, the time-averaged flow (figure 24*a* below) indicates a

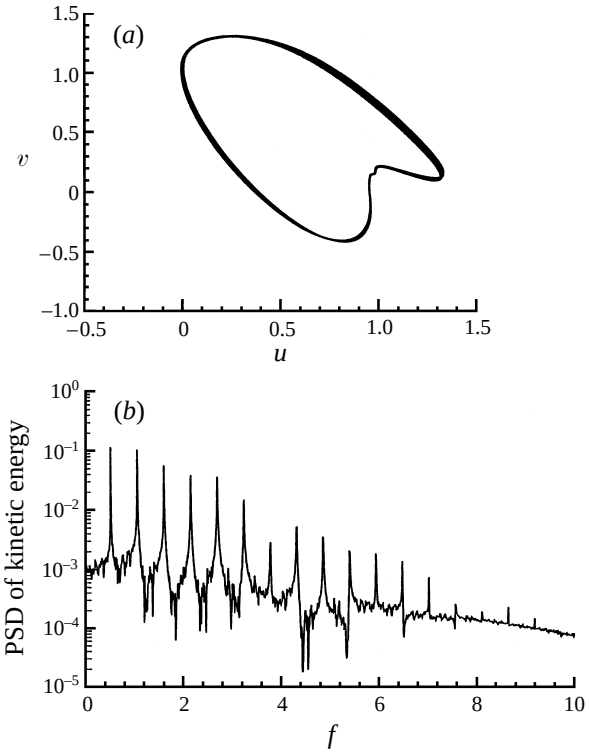

FIGURE 17. Instantaneous flow at point 3. $\alpha = 20°$, $\widehat{f}_e = 1$.

downwash. This may serve as an alternative explanation of the lift enhancement by appropriate forcing.

It is mentioned in § 4.2 that the forced vortex shedding causes a stronger impulse than the unforced one, which may be one of the reasons for the surface pressure to have larger amplitude on the front part of the airfoil. The present comparison of the structure of forced and unforced vorticity contours is consistent with this assertion.

As $\widehat{f}_e$ is increased to 2.0, the size and strength of both the lifting vortex and trailing-edge vortices are reduced (not shown). The doubling of forcing frequency implies that vortex merging near the leading edge occurs at a smaller scale than before, and so does the trailing-edge vortex formation. Therefore, the wake is narrower. It seems that the forcing at this f_e can take very good care of both high-frequency shear layer and low-frequency shedding. Two lifting vortices with a nice circular shape may coexist above the wing, and the unfavourable interference of the trailing-edge vortex is further limited. The wake vortices also align in a single array but the strength of vortex couples is halved and their spacing is more even. This further explains why the amplitude of C_l, C_d and C_p is greatly reduced.

The favourable effect of forcing declines as $\widehat{f}_e$ further increases to 4.0 (figure not shown), where we have $f_e/f^0_{shear} = 0.606$ which is of order one. Thus, as explained by Ho & Nosseir (1981), the shear layer is simply discretized to a series of travelling vortices; no rolling-up coalescence happens. Note that, in contrast to the case of $\widehat{f}_e = 2.0$, although we still found that the number of leading-edge vortices is doubled and their strength is halved, this is *not* the case for the trailing-edge vortex. Meanwhile, the small travelling vortices are not strong enough to entrain most of disorganized

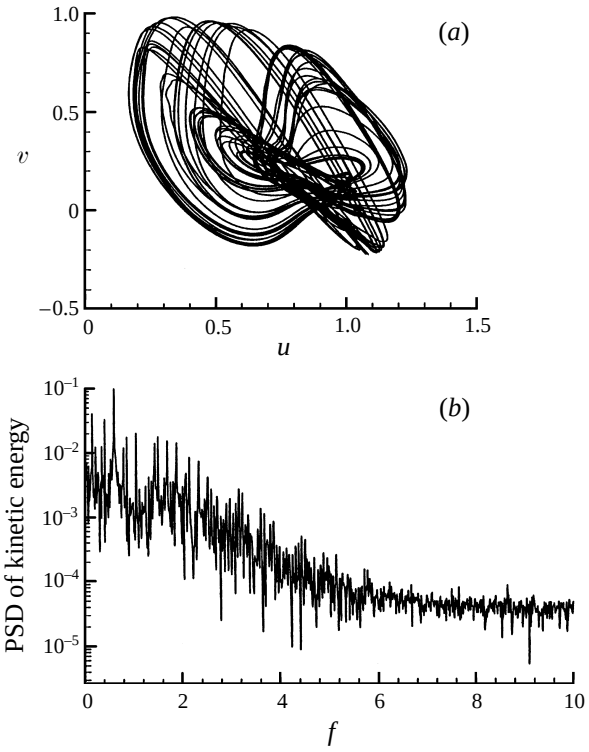

FIGURE 18. Instantaneous flow at point 3. $\alpha = 20°$, $\widehat{f}_e = 2$.

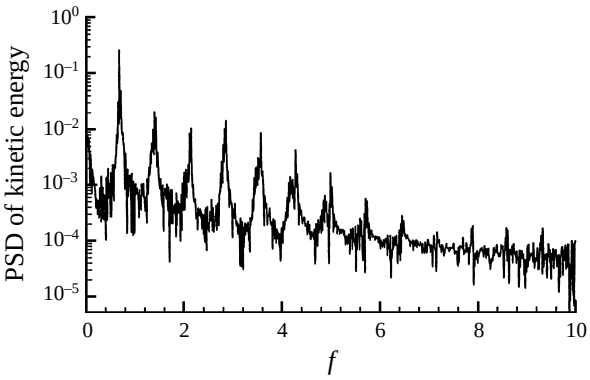

FIGURE 19. Instantaneous flow at point 3. $\alpha = 20°$, $\widehat{f}_e = 4$.

fluid. Consequently, the response shedding frequency no longer follows f_e, and the irregular secondary and tertiary separation reoccur. As a result, the drag is still reducing but the lift enhancement is small.

We mention that, without a turbulence model, the flow was found to separate earlier than with the B–L model (figure not shown). A series of small separated vortices appeared upstream and downstream of the forcing location, which did not merge to larger vortices. Therefore, in both unforced and forced cases, the oscillating flow patterns were less regular than those with a turbulence model.

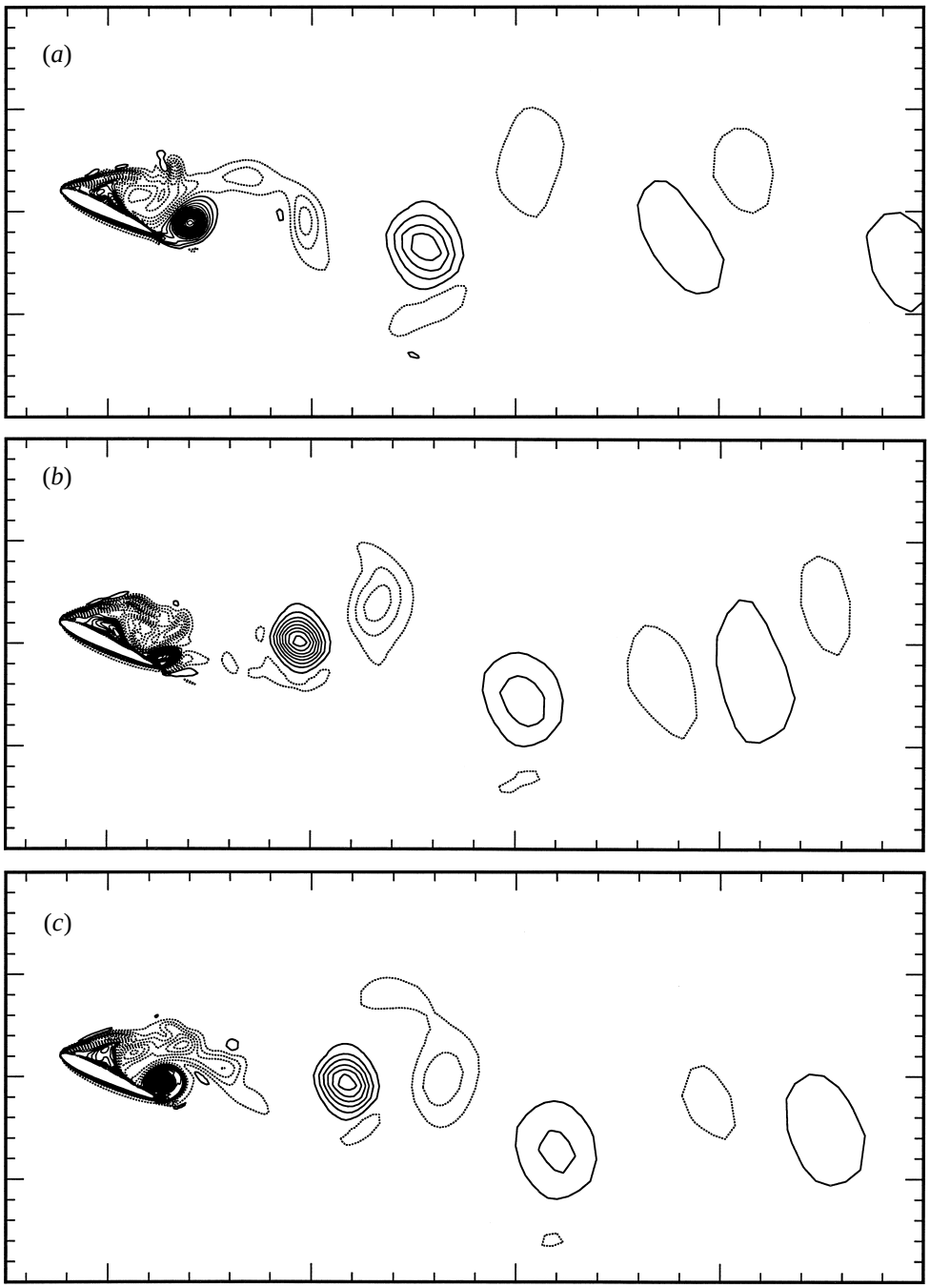

FIGURE 20. Instantaneous vorticity contours with constant time interval. Solid lines: $\omega > 0$, dotted lines: $\omega < 0$. $\alpha = 25°$, unforced.

6.2. *Time-averaged flow patterns*

The time-averaged streamlines and vorticity contours of unforced flow are shown in figure 23, indicating how much the lifting vortex is pushed up by its induced secondary separated vortex. This high position of the lifting vortex in turn induces

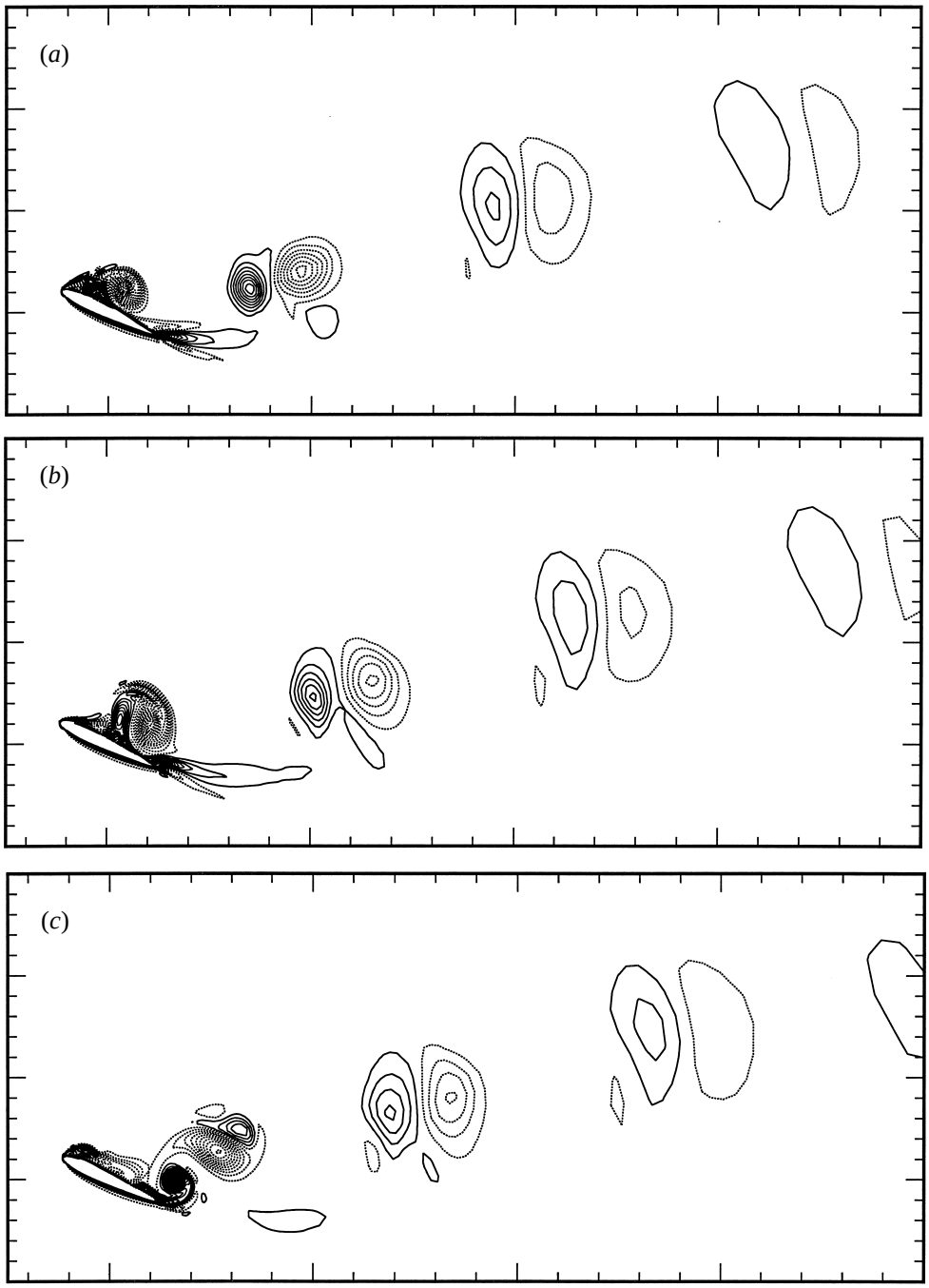

FIGURE 21. Instantaneous vorticity contours with the same constant time interval as in figure 20. Solid lines: $\omega > 0$, dotted lines: $\omega < 0$. $\alpha = 25°$, $\widehat{f}_e = 1$. The flow is periodic. Four frames almost form a period.

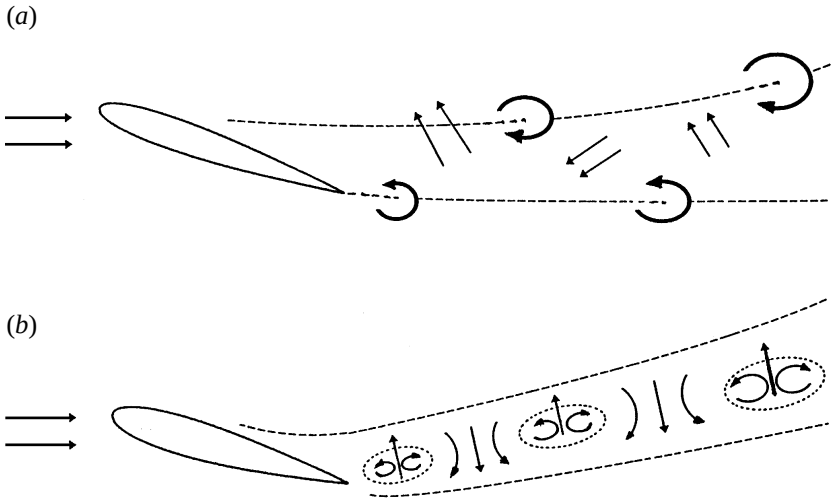

FIGURE 22. Sketch of the wake patterns. (*a*) $\widehat{f}_e = 0$. (*b*) $\widehat{f}_e = 1$.

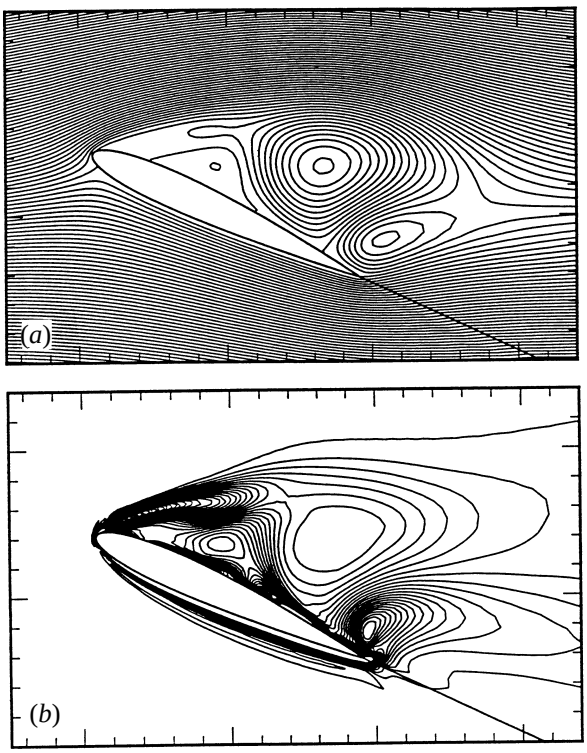

FIGURE 23. Time-averaged streamlines (*a*) and vorticity contours (*b*). $\alpha = 25°$. Unforced.

the trailing-edge vortex to invade deeply upstream and influence a large rear portion of the airfoil.

By contrast, figures 24 and 25 are the time-averaged streamlines and vorticity contours with $\widehat{f}_e = 1$ and 2 (when $\widehat{f}_e = 4$ the patterns become about the same as unforced case). It is evident that the mean lifting vortex is now in a much neater and

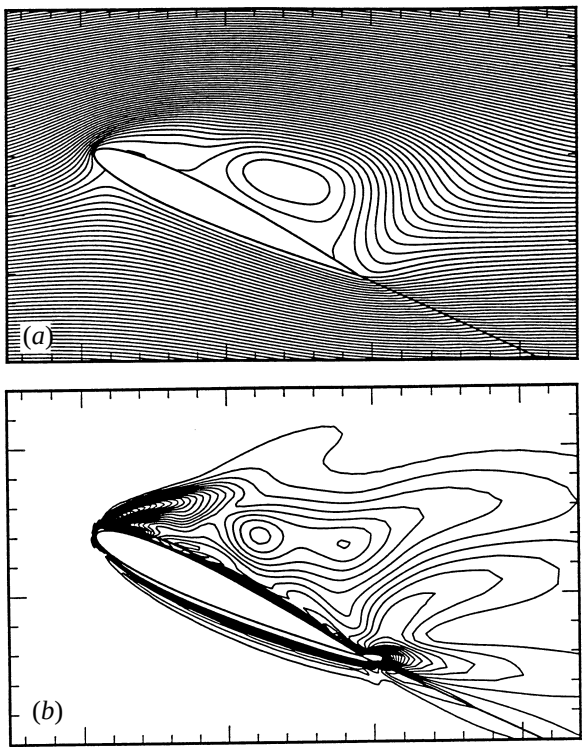

FIGURE 24. Time-averaged streamlines (*a*) and vorticity contours (*b*). $\alpha = 25°$, $\widehat{f}_e = 1$.

more comfortable circumstance, while the trailing-edge vortex is limited to a narrow fan region downstream the airfoil. Note that the two or three 'leaves' of the mean trailing-edge vorticity contours indicate that, before shedding off, the trailing-edge vortex wanders around the edge and stays longer at these positions in a period. When $\widehat{f}_e = 2$, the mean shear layer has very smooth contours. It extends across the whole chord length, basically parallel to the free stream with an almost constant mean thickness. The mean trailing-edge vortex is thereby pushed more downstream and confined in a even smaller region than that for $\widehat{f}_e = 1$. This nearly perfect resonant state at $\widehat{f}_e = 2$ results in a narrower wake and smaller drag.

In § 4.2 we noticed that the surface-pressure fluctuation near the trailing edge is greatly suppressed by forcing but did not give an explanation. We believe that this effect should be mainly attributed to the very favourable reduction of the trailing-edge vortex in both size and influence on the airfoil surface. Unlike the lift, this effect is stronger as f_e increases.

Note that the mean-streamline patterns satisfy the topological rule for two-dimensional cross-sectional flow (Hunt *et al.* 1978):

$$\left(\sum_N + \frac{1}{2}\sum_{N'}\right) - \left(\sum_S + \frac{1}{2}\sum_{S'}\right) = -1,$$

where N, N', S, and S' stand for node, semi-node, saddle, and semi-saddle, respectively. In figure 23(*a*) we have $\sum_N = 3$, $\sum_{N'} = 0$, $\sum_S = 1$, and $\sum_{S'} = 6$; while in figures 24(*a*) and 25(*a*), these numbers are 1, 0, 0, 4, respectively. The fewer the number of critical

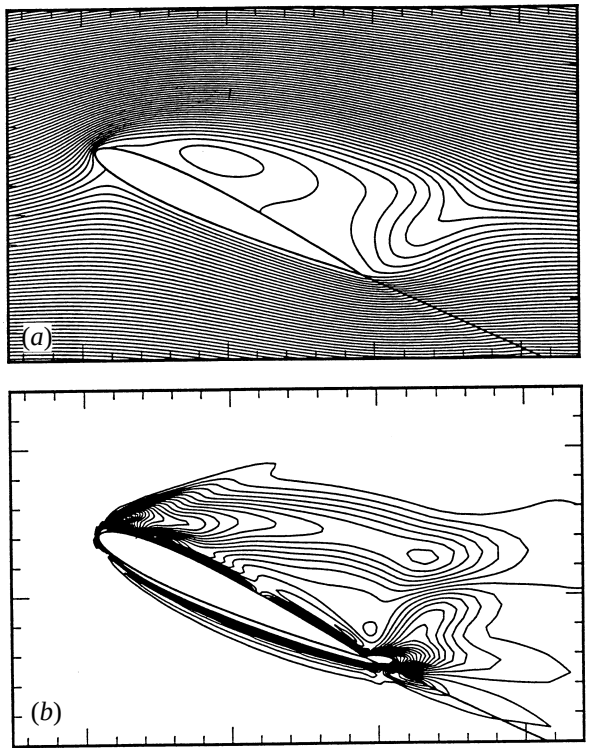

FIGURE 25. Time-averaged streamlines (*a*) and vorticity contours (*b*). $\alpha = 25°$, $\widehat{f}_e = 2$.

points, the 'healthier' would be the flow pattern – it would be easier to utilize and control. The post-stall resonance between the leading-edge shear layer and trailing-edge vortices, triggered by a low-level forcing, precisely achieves such a goal.

6.3. *Forced rolling-up coalescence and entrainment*

From the above discussion and recalling the results, we may interpret the main vortex-dynamics mechanisms that cause the difference between forced and unforced flow patterns as follows.

First, the forcing with a low frequency such as $f_e = f^0_{shed} = 0.152 f^0_{shear}$ at $\alpha = 25°$ causes several small discrete vortices, formed from high-frequency shear-layer instability, to quickly merge into a large vortex. In addition, we mention that a forcing with $c_\mu < 1\%$ did not enhance the lift in that case, i.e. the forcing strength must be above a threshold level. Therefore, we identify the vortex merging as a typical *rolling-up coalescence* addressed by Ho & Nosseir (1981). From computed vorticity contours, a merging of three vortices can be recognized. It was also observed that, compared to $\widehat{f}_e = 1.0$, when $\widehat{f}_e$ reduces to 0.5 the rolling-up coalescence involves more vortices and produces a larger vortex with higher strength (not shown); thus the maximal lift enhancement occurs at the low effective frequency end.

Secondly, since the main vortex has a rolling-up structure, when it is strong enough it will have the ability of *entraining* most disordered fluid into its core. This seems to be the fluid-dynamic mechanism of frequency lock-in for this special flow. Note that for two-dimensional steady flow without a sink of mass, the rolling-up is impossible. Here we see another unique advantage of unsteady control.

Thirdly, the entrainment by a strong lifting vortex is asymmetric on its upper and lower sides: the main entrainment occurs on its upper side, where the fresh stream brings larger momentum into the vortex, making it tend to turn downward. This is a very favourable effect. Since most of disorganized secondary and tertiary separated flow disappears, once saturated, the main vortex tends to be advected along the main stream direction, closer to the airfoil surface than the unforced case. Therefore, the upstream invading of trailing-edge vortices due to the induction of the main vortex travelling above it, as in the unforced case, is also greatly suppressed. The circulation around the airfoil is thus more favourable.

We stress that the first and second mechanisms, i.e. the rolling-up coalescence and strong entrainment, are both necessary. For example, even if the coalescence appears, the vortex formed thereby could be too far from the airfoil surface so that it cannot entrain most disorganized fluid. In this case the flow field will still behave like an unforced flow. This indeed happens at $\alpha = 30^\circ$ as was observed from the PSDs of some typical points (figures not shown). The remaining strong disorganized flow will conversely make the coalescence process aperiodic. This is the main reason for the observed much smaller lift enhancement.

7. Concluding remarks

The present study provides numerical evidence for post-stall flow control by unsteady excitation. The lift is increased (never decreased as noticed in experiments). If the forcing frequency is in an appropriate range, the drag, as well as the fluctuating amplitudes of lift and drag, can be reduced. The broadband random spectrum of surface-pressure fluctuation becomes a sharp-peak regularized spectrum, and near the trailing edge the fluctuating amplitude is drastically reduced.

For the NACA-0012 airfoil, the following items of our numerical results are in qualitative agreement with experiments on different airfoils by Hsiao's group and Zhou and Fernholz (see references cited in § 1): the range of angles of attack (20°–30°) within which a local unsteady forcing works; the forcing location (near the leading edge); the range of effective forcing frequency (about 0.3–2.0 f_{shed}); and the level of lift enhancement (up to 70%). Our computations also revealed some new phenomena that need be tested by future experiments. Unfortunately, due to the coexistence of several different flow regimes at post-stall angles of attack and the sensitivity of flow patterns to airfoil geometry, further quantitative comparison of our results with existing experiments does not make much sense. Nevertheless, along with these experiments, it can be asserted with confidence that the control effect does exist and could be very beneficial.

If the post-stall flow control can be further improved by adding a high-frequency forcing and/or sweeping the wing, then a monotonic increase of lift is possible for the whole range of $0 \leqslant \alpha \leqslant \alpha_m$, such that one can enjoy a new freedom to use the vortical lift on a wing or flap at a very high angle of attack, with the flow being completely separated. The post-stall control greatly enhances such a vortical lift.

The physical mechanisms behind the post-stall flow control by unsteady forcing are discussed based on our numerical solutions of Reynolds-averaged Navier–Stokes equations. For such a flow without forcing, both the local shear-layer instability and the global vortex shedding instability take place, each of which has a characteristic frequency. Their nonlinear interaction appears as mode competition, and sum and difference frequencies. It results in a complicated chaotic unsteady flow.

The nonlinear resonance between the unsteady excitation near the leading edge

and the separated shear layer thereof, and that between the same forcing and vortex shedding, play a key role in modifying the flow pattern. In a wide range of angles of attack, a forcing with appropriate frequency and amplitude can cause the response frequencies of both shed vortices and shear layer to lock into the harmonics of the forcing frequency, while other random modes are suppressed. In this way, the originally disorganized flow becomes a well organized flow.

From the vortex-dynamics point of view, the above organizing process corresponds to a sufficiently strong entrainment due to the rolling-up structure of the lifting vortex. To produce such an organized flow with high lift, there are some necessary conditions. First, the discrete vortices formed from the shear layer must be forced into rolling-up coalescence, which is possible only if the forcing frequency is an order lower than the natural shear-layer frequency, and the forcing amplitude is above a threshold. Secondly, the concentrated lifting vortex must be not too far from the airfoil surface. To ensure these conditions, the angle of attack cannot be too close to the stall angle, neither can it be too large.

Mainly due to the wide response spectrum of the shear layer to disturbances, different forcing frequencies result in different resonant states, which are responsible for different lift and drag characters. At the lowest tested forcing frequency (1/3 of the natural shedding frequency), the lifting vortex formed from rolling-up coalescence is strongest, giving rise to an optimal lift enhancement. Above this, there is a forcing frequency that can take best care of both shear-layer and vortex shedding instabilities, so that the entrainment effect is strongest and the flow is most organized, associated with a much narrower wake and smaller amplitude of fluctuating lift, drag, and surface pressure. Somewhere in between these two frequencies, the lift/drag ratio can be optimal. Further increasing the forcing frequency will no longer maintain the shedding frequency lock-in, and the flow returns to chaotic, associated with a reduction of the forcing effect.

To conclude this paper, we briefly discuss the specific circumstances where the post-stall flow control technique may be very useful. As said before, from the viewpoint of aerodynamic efficiency in the cruise condition, the optimal use of $L = -\rho U \Gamma$ is in the regime of attached flow. Any flow control cannot change this basic fact. However, just like the steady detached-vortex flow on slender wings or leading-edge extensions has greatly enlarged the range of usable angles of attack, we now expect that the unsteady controlled separated flow could be used at even larger angles of attack, as long as the drag is not a key issue to address. In practice, this happens at least in the following cases: (i) landing of aircraft with flap deployed; and (ii) highly manoeuvring flight.

In the first case, the technique can be applied to a flap as suggested by R. M. Wlezien (1996, private communication). The increased drag on the flap at post-stall angle of attack is only a small portion of the aircraft drag, which is beneficial in landing. The use of post-stall control would reduce the flap size and weight by enlarging its usable angle of attack. In the second case, the technique could be used on the main wing, for which a sharp-turn manoeuvre needs a large drag. It is worth exploring if the post-stall lift enhancement and buffet alleviation by unsteady control can be applied not only to large-aspect-ratio wings but also to slender wings.

The present work was supported in part by NASA Langley Research Center under the Grant NAG-1-1612. The authors are very grateful for the understanding and encouragement of Dr D. Dowyer and Mr W. L. Sellers, III, as well as help from our Technical Monitor, Dr R. D. Joslin. We appreciate very much the valuable discussions

with Drs M. D. Zhou, D. P. Telionis, D. G. Crighton, R. W. Wlezien, V. K. Sharma, and Mr J. H. Hogue. We also thank Dr R. Roach who provided us with the original VNS code, and Mr F. L. Zhu who conducted some numerical tests. The second and fourth authors (X. Y. L. and M. F.) would like to thank the support of the J. M. Wu Research Fund of the University of Tennessee Space Institute during their visit to UTSI. M. F. was also supported in part by Peking University, China.

REFERENCES

Baldwin, B. S. & Lomax, H. 1978 Thin layer approximation and algebraic model for separated turbulent flows. *AIAA Paper* 78-257.

Barton, J. T. & Pulliam, H. 1984 Airfoil computation at high angles of attack, inviscid and viscous phenomena. *AIAA Paper* 84-0524.

Batchelor, G. K. 1956 Unsteady laminar flow with closed streamlines at large Reynolds number. *J. Fluid Mech.* **1**, 177–190.

Chang, R. C., Hsiao, F.-B. & Shyu, R.-N. 1992 Forcing level effects of internal acoustic excitation on the improvement of airfoil performance. *J. Aircraft* **29**, 823–829.

Chernyshenko, S. I. 1995 Stabilization of trapped vortices by alternating blowing–suction. *Phys. Fluids* **7**, 802–807.

Chernyshenko, S. I. & Castro, I. P. 1993 High-Reynolds-number asymptotics of the steady flow through a row of bluff bodies. *J. Fluid Mech.* **257**, 421–449.

Collins, F. G. & Zelenevitz, J. 1975 Influence of sound upon separated flow over wings. *AIAA J.* **13**, 408–410.

Cornish, J. J. 1982 Vortex flows. *8th Quick-Goethert Lecture Series, Oct. 21, 1982, Univ. Tenn. Space Inst.* Lockheed-Georgia Company.

Critzos, C. C., Heyson, H. H. & Boswinkle, R. W. 1955 Aerodynamic characteristics of NACA 0012 airfoil section at angles of attack from 0° to 360°. *NACA TN* 3361.

Denny, A. G. 1997 Numerical study of lift augmentation by mechanical forcing applied to massively separated turbulent flows. PhD Thesis, The University of Tennessee, Knoxville, TN.

Detemple-Laake, E. & Eckelmann, H. 1989 Phenomenology of Kármán vortex streets in oscillating flow. *Exps. Fluids* **7**, 217–227.

Fage, A. & Johansen, F. C. 1927 On the flow of air behind an inclined flat plate of infinite span. *Proc. R. Soc. Lond.* A **116**, 170–197.

Gerrard, J. H. 1978 The wakes of cylindrical bluff body at low Reynolds number. *Phil. Trans. R. Soc. Lond.* A **288**, 351–382.

Gharib, M. & William-Stuber, K. 1989 Experiments on the forced wake of an airfoil. *J. Fluid Mech.* **208**, 225–255.

Gillan, M. A. & Cooper R. K. 1994 Computational analysis of buffet alleviation over a porous airfoil at high angle of attack. *AIAA Paper* 94-1818.

Ho, C.-M. & Huang, L.-S. 1982 Subharmonics and vortex merging in mixing layers. *J. Fluid Mech.* **119**, 443–473.

Ho, C.-M. & Huerre, P. 1984 Perturbed free shear layers. *Ann. Rev. Fluid Mech.* **16**, 365–424.

Ho, C.-M. & Nosseir, N. S. 1981 Dynamics of an impinging jet. Part I. The feedback phenomenon. *J. Fluid Mech.* **105**, 119–142.

Hsiao, F.-B., Liu, C.-F. & Shyu, J.-Y. 1990 Control of wall-separated flow by internal acoustic excitation. *AIAA J.* **28**, 1440–1446.

Hsiao, F.-B., Shyu, R.-N. & Chang, R. C. 1994 High angle-of-attack airfoil performance improvement by internal acoustic excitation. *AIAA J.* **32**, 655–657.

Hsiao, F.-B., Wang, T.-Z. & Zohar, Y. 1993 Flow separation control of a 2-D airfoil by a leading-edge oscillating flap. *Intl Conf. Aerospace Sci. Tech., Dec. 6–9, 1993, Tainan, Taiwan.*

Huerre, P. & Monkewitz, P. A. 1990 Local and global instabilities in spatially developing flows. *Ann. Rev. Fluid Mech.* **22**, 473–537.

Hunt, J. C. R., Abell, C. J., Peterla, J. A. & Woo, H. 1978 Kinematical studies of the flows around free or surface mounted obstacles: applying topology to flow visualization. *J. Fluid Mech.* **86**, 179–200.

Jones, B. M. 1934 Stalling. *J. R. Aeronaut. Soc.* **38**, 753–770

Karniadakis, G. E. & Triantafyllou, G. S. 1989 Frequency selection and asymptotic states in laminar wakes. *J. Fluid Mech.* **199**, 441–469.

Ko, S. & McCroskey, W. J. 1997 Computations of unsteady separating flows over an oscillating airfoil. *AIAA Paper* 95-0312.

Koochesfahani, M. M. 1989 Vortical patterns in the wake of an oscillating airfoil. *AIAA J.* **27**, 1200–1205.

Koopmann, G. H. 1967 The vortex wakes of vibrating cylinders at low Reynolds numbers. *J. Fluid Mech.* **28**, 501–512.

Kourta, A., Boisson, H. C., Chassaing, P. & Minh, H. H. 1987 Nonlinear interaction and the transition to turbulence in the wake of a circular cylinder. *J. Fluid Mech.* **181**, 141–161.

Lam, K. M. 1996 Phase-locked reduction of vortex shedding in flow past an inclined flat plate. *Phys. Fluids* **8**, 1159–1168.

Lamb, H. 1932 *Hydrodynamics*. Cambridge University Press.

Launder, B. E. & Sharma, B. I. 1974 Application of the energy-dissipation model of turbulence to the calculation of flow near a spinning disc. *Lett. Heat Mass Transfer* **1**, 131–138.

Laurie, K. B. & Farokhi. 1993 Separated flowfield and lift on an airfoil with an oscillating leading-edge flap. *AIAA Paper* 93-3422.

Lu, X. Y. & Dalton, C. 1996 Calculation of the timing of vortex formation from an oscillating cylinder. *J. Fluids Structures* **10**, 527–541.

Lu, X. Y. & Sato, J. 1996 A numerical study of flow past a rotationally oscillating circular cylinder. *J. Fluids Structures* **10**, 829–849.

Malkus, W. V. 1996 Statistical stability criteria for turbulent flow. *Phys. Fluids* **8**, 1582–1587.

McMichael, J. M. 1996 Progress and prospects for active flow control using microfabricated electromechanical system (MEMS). *AIAA Paper* 96-0306.

Miksad, R. W., Jones, F. L., Powers, E. J., Kim, Y. C. & Khadra, L. 1982 Experiments on the role of amplitude and phase modulations during transition to turbulence. *J. Fluid Mech.* **123**, 1–29.

Olinger, D. J. & Sreenivasan, K. R. 1988 Nonlinear dynamics of the wake of an oscillating cylinder. *Phys. Rev. Lett.* **60**, 797–800.

Rockwell, D. O. 1972 External excitation of plan jets. *Trans. ASME* E: *J. Appl. Mech.* **39**, 883–890.

Rockwell, D. 1990 Active control of globally-unstable separated flows. *Intl Symp. Nonsteady Fluid Dynamics, June 4–7, 1990, Ontario, Canada.* (ed. J. A. Miller & D. P. Telionis) pp. 379–394, ASME.

Rumsey, C. L., Thomas, J. L., Warren, G. P. & Liu, G. C. 1987 Upwind Navier–Stokes solutions for separated periodic flows. *AIAA J.* **25**, 535–541.

Seifert, A., Bachar, T., Koss, D., Shepshelovich, M., & Wygnanski, I. 1993 Oscillatory blowing: a tool to delay boundary-layer separation. *AIAA J.* **31**, 2052–2060.

Seifert, A., Darabi, A. & Wygnanski, I. 1996 Delay of airfoil stall by periodic excitation. *J. Aircraft* **33**, 691–698.

Smith, B. L. & Glezer, A. 1997 Vectoring and small-scale motions effected in free shear flows using sythetic jet actuators. *AIAA Paper* 97-0213.

Spalart, P. R. & Allmaras, S. R. 1992 A one-equation turbulence model for aerodynamic flows. *AIAA Paper* 92-0439.

Stansby, P. K. 1976 The lock-on of vortex shedding due to the cross-stream vibration of circular cylinders in uniform and shear flows. *J. Fluid Mech.* **74**, 641–665.

Thompson, K. W. 1990 Time-dependent boundary conditions for hyperbolic systems, II. *J. Comput. Phys.* **89**, 439–461.

Unal, M. F. & Rockwell, D. 1988 On vortex formation from a cylinder. Part 1. The initial instability. *J. Fluid Mech.* **190**, 491–512.

White, F. M. 1974 *Viscous Fluid Flow*. 2nd Edn. McGraw-Hill.

Willam-Stuber, K. & Gharib, M. 1990 Transition from order to chaos in the wake of an airfoil. *J. Fluid Mech.* **213**, 29–57.

Williamson, C. H. K. 1996 Vortex dynamics in the cylinder wake. *Ann. Rev. Fluid Mech.* **28**, 477–539.

Wu, J. M. & Wu, J. Z. 1993 Vortex lift at a very high angle of attack with massively separated unsteady flow. In *Fluid Dynamics of High Angle of Attack* (ed. R. Kawamura & Y. Aihara), pp. 35–63. Springer.

Wu, J. Z. Ma, H. Y. & Wu, J. M. 1994 Viscous sound-vortex interaction in a duct shear flow. *J. Sound Vib.* **172**, 103–126.

Wu, J. Z., Vakili, A. D. & Wu, J. M. 1991 Review of the physics of enhancing vortex lift by unsteady excitation. *Prog. Aerospace Sci.* **28**, 73–131.

Wu, J. Z. & Wu, J. M. 1996 Vorticity dynamics on boundaries. *Adv. Appl. Mech.* **32**, 119–275.

Wu, J. Z., Wu, X. H. & Wu, J. M. 1993 Streaming vorticity flux from oscillating walls with finite amplitude. *Phys. Fluids* A **5**, 1933–1938.

Wu, X. H., Wu, J. Z. & Wu, J. M. 1991 Streaming effect of wall oscillation to boundary layer separation. *AIAA Paper* 91-0545.

Wygnanski, I. 1987 Coherent motion in excited free shear flows. *AIAA J.* **25**, 201–213.

Wygnanski, I. 1997 Boundary layer and flow control by periodic addition of momentum. *AIAA Paper* 97-2117.

Zaman, K. B. M. Q., McKinzie, D. J. & Rumsey, C. L. 1989 A natural low-frequency oscillation of the flow over an airfoil near stalling conditions. *J. Fluid Mech.* **202**, 403–442.

Zhou, M. D., Fernholz, H. H., Ma, H. Y., Wu, J. Z. & Wu, J. M. 1993 Vortex capture by a two-dimensional airfoil with a small oscillating leading-edge flap. *AIAA Paper* 93-3266.